공학석사학위논문

풍력발전 기어박스의 진동 기반 고장진단 프레임워크

Vibration-based framework for fault diagnostics of wind turbine gearbox

2013 년 08 월

서울대학교 대학원

기계항공공학부

하 종 문

진동 기반 풍력발전기 기어박스의 고장진단 프레임워크

Vibration-based framework for fault diagnostics of wind turbine gearbox

지도교수 윤 병 동

이 논문을 공학석사 학위논문으로 제출함

2013 년 08 월

서울대학교 대학원
기계항공공학부
하 종 문

이름 의 공학석사 학위논문을 인준함

2013 년 06 월

위 원 장 _____ 김 윤 영 _____ (인)

부위원장 _____ 윤 병 동 _____ (인)

위 원 _____ 김 도 년 _____ (인)

Abstract

Vibration-based framework for fault diagnostics of wind turbine gearbox

Jong Moon Ha
School of Mechanical and Aerospace Engineering
The Graduate School
Seoul National University

Reliability of wind turbines (WT) is a challenging issue in wind energy industry. In particular, a gearbox in a WT has the highest risk because of its high maintenance cost. Despite many prior attempts to develop diagnostics techniques for WTs, one has faced many grand challenges including 1) inaccuracy in fault diagnostics due to random and non-stationary signals and 2) inefficiency in fault diagnostics with big sensory data (e.g. vibration) from many sensors in a WT.

This study thus aims at developing a generic guideline and framework for gearbox fault diagnostics. This framework enables accurate diagnostic analysis while working with a massive volume of sensory data from many sensors in an efficient manner. This paper proposes two key ideas in the following research areas as: 1) classification of operational data, and 2) vibration-based fault diagnostics method. First, this study has classified the operation conditions into four non-trivial (Class I. stationary; Class II. quasi-stationary; Class III. non-stationary with high correlation; Class IV. non-stationary with no correlation) conditions and one trivial (Class V. idle) condition in terms of the operation data (rotor speed, and power) of the WTs. Data classification has been conducted with real operational data acquired from Young Heung wind

farms. Next, this study has also designed diagnostics methods for the first non-trivial class (Class I) based on the characteristics of the data classes. A core technique for the fault diagnostics is an order analysis method using Time Synchronous Averaging (TSA), where TSA is generally used for signal de-noising and the order analysis for the extraction of health data for a gearbox. It is, however, a daunting task to execute the fault diagnostics using the conventional TSA for a planetary gearbox because of multiple mesh contacts and rotation of the axes of planet gears. This paper proposes a new TSA idea, referred to as Autocorrelation-based TSA (ATSA) for the order analysis, particularly for a planetary gearbox.

For the demonstration of the proposed diagnostics framework, two signals were employed: analytical signals and signals from a WT testbed. A 2kW WT testbed was designed with two DC motors, main bearing, flywheel and gearboxes with 13 sensors. A faulty gear was machined with different crack lengths at the root of the gear mesh and assembled into the gearbox. The order analysis based on ATSA processed the signals acquired from the healthy and faulty gearbox. It was concluded that the proposed diagnostics method can distinguish the faulty condition of the gearbox from the healthy one.

Keywords: Wind turbine gearbox
Fault diagnostics
Planetary gearbox
Time synchronous averaging
Classification of operations data

Student Number: 2011-23346

Table of Contents

List of Tables

List of Figures

Nomenclatures

$F_c(\bullet)$	Inverse cumulative frequency function
x_k	Defined operation value
X_r	Operation data
N_{bins}	The number of bins
$I(\bullet)$	Indicator function
c_1	Starting point of range
c_2	Ending point of range
$N_{samples}$	The number of samples in the region
$v(\bullet)$	Synthesized signal
$S(\bullet)$	Synchronous coherent signal
$N(\bullet)$	Non-synchronous coherent signal
$R(\bullet)$	Non-coherent random signal
f_{re}	Resampling frequency
t_n	Time of n^{th} sample
θ_n	Angle of n^{th} sample
t^*_n	Time of n^{th} sample after resampling
θ^*_n	Angle of n^{th} sample after resampling
$\overline{S(\bullet)}$	Estimation of synchronous coherent signal

$N_{ensemble}$	The number of ensemble sets
N_s	The number of teeth in sun gear
N_p	The number of teeth in planet gear
N_r	The number of teeth in ring gear
f_{LSS}	Rotational frequency of low speed shaft
f_{HSS}	Rotational frequency of high speed shaft
f_s	Rotational frequency of sun gear
f_p	Rotational frequency of planet gear
f_c	Rotational frequency of carrier
f_{pr}	Rotational frequency of planet gear relative to ring gear
f_{ps}	Rotational frequency of planet gear relative to sun gear
f_{GMF}	Frequency of fundamental gear mesh
$P_{n_c,p}$	Teeth sequence of planet gear at n_c rotation of carrier
n_c	The number of rotation of carrier
$n_{Rest,\mathrm{p}}$	Hunting tooth ratio
$LCM(\bullet)$	Least common multiple
HTR_c	Hunting tooth ratio of carrier
t	Time
τ	Time lag
$R_{vv}(\bullet)$	Sample autocorrelation function

n_{pr}	Rotation of planet gear relative to ring gear
$\mu_{(\bullet),\,i}$	i^{th} statistical moment of target signal
$x_{(\bullet)}$	Data from target signal
$\overline{x_{(\bullet)}}$	Average of target signal
$\sigma_{(\bullet)}$	Standard deviation of target signal
$A(f_i)$	Amplitude of i^{th} fundamental frequency
$A(s_j^{\,f_i})$	Amplitude of j^{th} sideband centered on i^{th} fundamental frequency
Z	Z-value (statistics)
E	Energy of Hilbert transform
$H[\bullet]$	Hilbert transform
v_p	Vibration from one planet gear
P	The number of planet gears
a_{pi}	Transfer factor of i^{th} planet gear
$noise_i$	Noise factor of i^{th} planet gear
V_{rand}	Random value from 0 to 1
A_{noise}	Amplitude of averaging noise
$A_{noise,min}$	The minimum of amplitude of noise

Chapter 1. Introduction

1.1 Motivation

One of the most significant current issues in the world is converting to sources of renewable energy for the purpose of reduction in global CO_2 emissions and overcoming exhaustion of energy. Among the various renewable energy sources, wind energy is considered one of the most promising because its efficiency. Thus, the market size of the wind industry has increased at an astonishing rate in recent years. Global cumulative installed wind capacity had reached 250 GW by 2012, and the Global Wind Energy Council (GWEC) estimates that global cumulative installed wind capacity will exceed 1600 GW by 2030 [1]. The International Energy Agency (IEA) estimated that energy from the rapidly growing wind farm industry will be able to cover 12 % of global electricity needs by 2050 [2]. Moreover, the COE (Cost of Energy) of a wind turbine (WT), which is one of the most significant values used to evaluate the efficiency of energy, is predicted to be reduced by 23 % by 2050 [2]. This means there is no doubt that wind energy is having considerable impact as a sustainable and renewable energy and the industry has potential to impact world-wide energy on an even larger scale in the coming years.

COE of WTs can be effectively reduced by decreasing Operation & Maintenance (O&M) costs. In particular, reduction of O&M cost is a significant consideration in the case of offshore WTs because offshore WTs have higher O&M costs than onshore WTs. Y. Feng et al. compared several papers about reliability of wind farms and found that O&M costs account for 18% of total COE in offshore

WTs, and 12% in onshore WTs [3]. O&M costs can be substantially reduced by diagnosing and predicting potential faults in WTs. David McMillan et al. studied the benefits from condition-based maintenance by using diagnostics tools and concluded that proper use of diagnostics for offshore WT is estimated to save 76,784£ per offshore WT per year [4]. Thus, fault diagnostics is an essential part of the WT and has been widely developed by many researchers.

Despite extensive efforts in the diagnostics researches, we are still confronted with many grand challenges for developing diagnostics tools for WTs such as : 1) random non-stationary signals and 2) massive amount of data. Most WTs operate in heavily random and non-stationary. This necessitates the use of time-frequency analysis. Because of intense computation required by the analysis of a massive amount of sensory data under random non-stationary condition, however, it is prohibitively used for diagnostics of WTs in real-time. Spectral analysis based on time synchronous averaging (TSA) were generally used for diagnostics of the gearboxes of helicopter because of their efficiency in computation. Despite the efficiency, it is difficult to be applied to the WT because they require huge amount of stationary signals which is rarely acquired in the WTs. Moreover, there is no guideline where to use spectral analysis and where to use time-frequency analysis for computational efficiency and robust analysis.

To solve these practical issues, a generic guideline and fault diagnostics framework which involves classification of wind data and diagnostics using order analysis based on Autocorrelation-based Time Synchronous Averaging (ATSA) is proposed in this thesis.

1.2 Scope of research

This thesis proposes two key ideas in the following research area as: 1) classification of operational data and 2) vibration-based fault diagnostics of the WT gearbox.

using order analysis based on Autocorrelation-based Time Synchronous Averaging (ATSA).

In the research thrust 1, classification of wind data, the huge amount of response (e.g. vibration) data is classified into four non-trivial (Class I. stationary; Class II. quasi-stationary; Class III. non-stationary with high correlation; Class IV. non-stationary with no correlation) conditions and one trivial (Class V. idle) condition in terms of the operation data (rotor speed, and power) of the WTs. And then optimal diagnostics plans are designed for each class. As a result, trivial class is filtered out and only non-trivial classes are adaptively extracted for the purpose of diagnostics. This procedure makes it possible to manage big data efficiently and utilize only meaningful data for fault diagnostics. Among the classes, it is found that defined class I and II are appropriate for the diagnostics tool developed in research thrust 2.

In research thrust 2, this study has also designed diagnostics methods for the first non-trivial class (Class I & II) based on the characteristics of the data classes. A core technique for the fault diagnostics is an order analysis method using Autocorrelation-based Time Synchronous Averaging (ATSA), where ATSA is used for signal de-noising and the order analysis for the extraction of health data for a gearbox. Then, current health state of the WTs can be estimated from various health data which are calculated from the order domain.

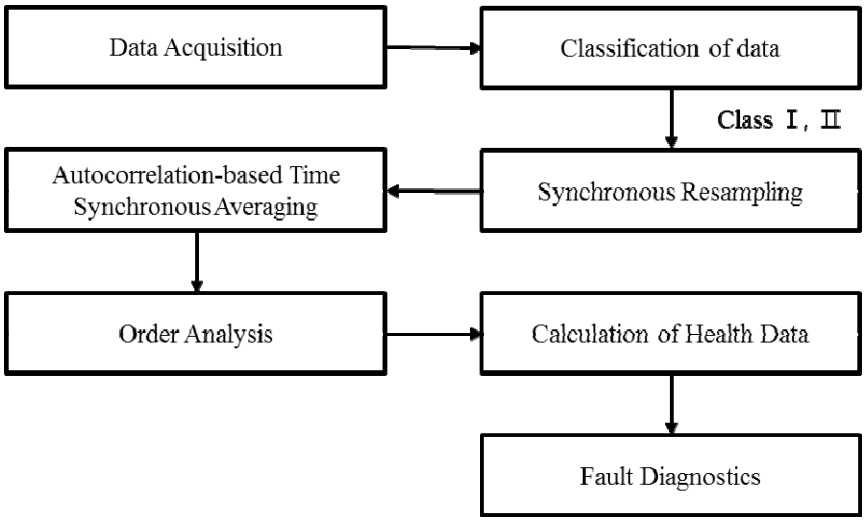

Figure 1-1 Framework for fault diagnostics of WT gearboxes

1.3 Structure of the Thesis

In Chapter 2, condition monitoring methods are briefly reviewed. Chapter 3 presents classification of operational data. Chapter 4 summarizes the TSA method and develops ATSA. In Chapter 5, the various health data for WT gearbox that can be obtained from vibration signals are reviewed and summarized. Among them, a few types of health data will be used for validation of the diagnostics techniques proposed in this paper. Chapter 6 involves design of analytical signals the WT testbed for validation, and corresponding analysis results are presented. Chapter 7 summarizes the research and presents the conclusions of the thesis.

Chapter 2. Review of Condition Monitoring

Condition monitoring can be performed in two ways: 1) SCADA (supervisory control and data acquisition system) based condition monitoring and 2) vibration based condition monitoring. In this section, a brief overview of the two condition monitoring methods is presented.

2.1 SCADA-based Condition Monitoring

SCADA (supervisory control and data acquisition system) consists of three kinds of data, including environmental data, operational data, and response data, as summarized in Table 2-1. It was originally designed to supervise and control power plants based on the plant's operational and environmental conditions. Operational data from individual WT systems are collected from sensors attached to the systems, then overall information of the power plant is supervised comprehensively in a central processing unit. Data are collected at a very low frequency, for example once every 10 minutes, to make it possible to manage a huge power plant in real-time.

D. Z. Chen and Bindi studied commercially available SCADA systems which are embedded in real wind farms and summarized the main features of those systems [5]. They found that most SCADA includes not only the plant management functions but also basic condition monitoring units such as alarm management systems. Condition monitoring using SCADA can be divided into two main subjects: monitoring of power [6], [7] and monitoring of temperature of the main

components such as gearbox, generator winding and bearing [8], [9], [10]. Furthermore, principal concepts of other studies are mainly estimation of the normal state and monitoring the current state of the system using several parameters such as ambient temperature, rotating speed and so on as well as the power and the temperature of the main components. PCA (Principal Component Analysis) [6], NN (Neural Network) [10], AARK (Auto-associative Kernel Regression) [9], and NSET (Nonlinear State Estimate Technique) [8] are widely used for this purpose.

Table 2-1 SCADA data from wind turbines

Data Type	Description
Environmental data	Wind Speed & direction
	Outside temperature
Operational data	Power output
	Rotor speed
	Control logic (Yaw, Pitch, Idle, and etc.)
	Messages about interventions in the control of the turbine
Response data (Vibration)	Nacelle vibrational response
	Bearing vibration
	Gearbox vibration
	Generator vibration
Response data (Temperature and etc.)	Nacelle temperature
	Temperature of bearings of gearbox and generator
	Temperature of the generator windings
	Oil temperatures and pressure

Unfortunately, the accuracy is not reliable because of the low sampling rate of SCADA. However, condition monitoring using SCADA is very important because it provides a basic guideline for thorough investigation of the system.

2.2 Vibration-based Condition Monitoring System(CMS)

A condition monitoring system (CMS) is an essential part of the wind turbine (WT). GL, one of the most significant organizations involved in the certification of WT systems, enacted a regulation that every system should be equipped with a condition monitoring system which uses high-frequency response data (e.g., vibration) rather than SCADA[11]. In this section, vibration-based CMS techniques are briefly reviewed.

2.2.1 Spectral Analysis

As stated in Chapter 1, we are confronted with an inevitable challenge: the large amount of data. To overcome this challenge and realize real-time diagnostics of WT, most commercially available CMS are equipped with cost-efficient methods such as time domain analysis and spectral analysis with FFT (Fast Fourier Transform) [12]. Time domain analysis is the most basic condition monitoring tool which utilizes the level of amplitude, statistical moments and some features like instant peak of vibration signal in time axis. C. J. Crabtree et al. (2010) traced the level of vibration signal along with applied load to detect incipient failure of a WT gearbox [13]. However, time domain analysis is rarely used alone for CMS and

several studies have shown that spectral analysis can be used with time domain analysis. Spectral analysis is composed of three stages: the de-noising stage, the transformation to frequency domain stage, and the analysis of spectral component stage.

The de-noising stage is required especially in real-world field settings where signals typically include considerable random noise. This is also known as the pre-processing stage. High-pass filtering and time synchronous averaging (TSA) [14] are widely used in this stage. TSA is adopted and revised in this paper for de-noising; details will be given in Chapter 4.

Next, pre-processed signals need to be transformed to the frequency domain through a transformation stage. FFT (Fast Fourier Transform) is widely used for this procedure [15]; however, FFT requires signals under both cyclic and stationary state. Windows functions such as Hamming window can be used to decrease the negative effects of non-cyclic signals but there are limitations when signals are non-stationary [16]. A resampling technique can be applied to overcome the small non-stationary condition. This technique will be presented as a part of the diagnostics framework in Chapter 4.

Health data can be extracted by calculating statistical indices of specific components from the frequency domain, and this overall procedure is performed in analysis of the spectral component stage. Several health data related to WT gearboxes will be reviewed and summarized in Chapter 5.

2.2.2 Time-frequency analysis

Time domain analysis and spectral analysis have advantages in that these

techniques are computationally efficient. However another challenge arises here because most WTs operate in non-stationary conditions which make it difficult to use these techniques for condition monitoring of WT. So, there have been many attempts to develop more accurate condition monitoring techniques under non-stationary conditions, such as time-frequency analysis.

FFT loses time information as the signal is transformed into the frequency domain. STFT (Short Time Fourier Transform) is the most basic time-frequency analysis method which uses the basic principle of FFT while considering time information [17]. The local window function is defined to cover only a short time of the whole signal; this window moves along with time. FFT is applied to every windowed signal and time information is stored as the window function is shifting. As a result, STFT becomes a function of both time and frequency. However, resolution of frequency and time of the STFT cannot be simultaneously fine because the window function of STFT is not time for frequency varying but deterministic function.

To overcome this challenge, wavelet transform was developed to have an adaptive window (i.e. Mother function) function which is dilated and shifted corresponding to characteristics of signal [17]. Wavelet transform have been widely studied for diagnostics of WT under non-stationary condition [18]. However, accuracy of the analysis cannot be guaranteed when the signals have mostly non-linear behavior.

Empirical mode decomposition (EMD) was developed by N. Huang to deal with non-linear signals as well as non-stationary signals by decomposing the signal into several Intrinsic Mode Functions (IMFs) [19]. EMD is widely used in diagnostics of WT because most WT operates in non-stationary condition because of non-linear

behavior of the wind [20]. Various further research on EMD for the purpose of diagnostics of the WT, such as Bivariate empirical mode decomposition (BEMD) and ensemble empirical mode decomposition (EEMD), have been actively studied [21], [22].

Chapter 3. Classification of Operation Data

Equation Section 3

3.1 Introduction

SCADA consists of three kinds of data, including environmental data, operational data, and response data, as summarized in Table 2-1. Response data, especially vibration signals, occupy most size of the data. Because of the difficulties in dealing with such big data, simple diagnostics methods such as order analysis are widely used in diagnostics of real WT. However, WTs mostly operate in non-stationary conditions. This makes it extremely difficult to accurately analyze the signals under non-stationary condition and it leads to the need for better techniques such as time-frequency analysis; however, this technique is too computationally intensive to be practical. Thus, efficient data management method and the guideline which helps to determine where to use the order analysis and where to use the time-frequency analysis are needed to overcome such practical issues. This paper thus attempts to develop diagnostics framework which includes the method for classification of operation data of WT, and design of the corresponding diagnostics methods for each class. A distinction between trivial and non-trivial classes is made in an effort to reduce the size of data and optimal diagnostics methods are designed based on characteristics of signal under the defined classes. Operational data collected from a SCADA of a WT for 7 months was used for this study. Among various information available from SCADA, power output and rotor speed is adopted for classification. At the end, corresponding diagnostics methods are suggested for each class.

3.2 Classification Method

Classification employs two operational data – rotor speed and generated power. A rule of thumb for the classification is to understand the natures of turbine operation states because different states require different health monitoring strategies.

Figure 3-1 helps to understand the behavior of WTs by graphically describing rotor speed and generated power, along with time. Wind speed is also presented for further understanding of the data. The main role of a WT is to generate high power under given conditions. Thus, a WT is basically designed to have a high correlation between rotor speed and power output. As you can see in Figure 3-1, class I corresponds to a stationary state because the rotor speed and power remain nearly unchanged at maximum. However, the expected correlation between rotor speed and power output is not guaranteed at all times. Generated power can fluctuate, even with unchanged rotor speed. This region is

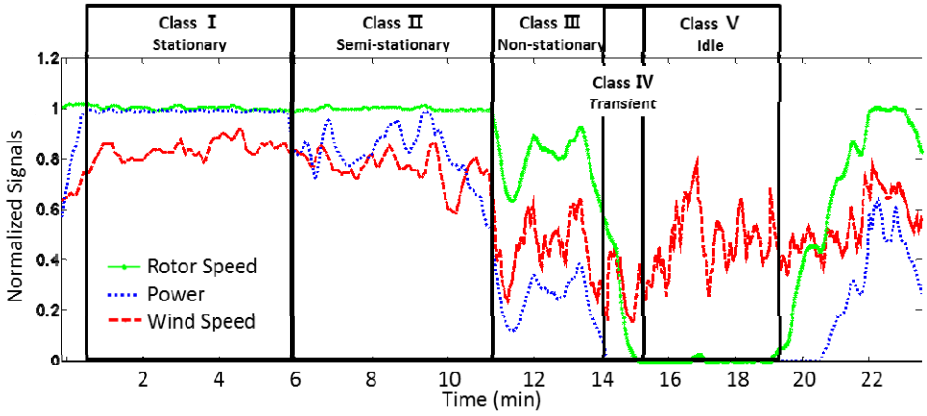

Figure 3-1 Classification of wind data using graphical method

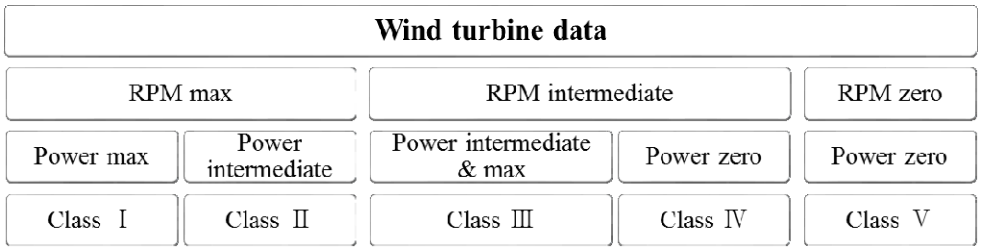

Figure 3-2 Classification method

defined as class II, the quasi-stationary state. Classes III and IV fall into a non-stationary state because both RPM and power change over time. Data in class III can be characterized with a high statistical correlation between rotor speed and power whereas the data in class IV cannot because this is the transient region. During class V, the WT is idling. Figure 3-2 shows the classification method.

The following sections will explain the method developed to classify the data in a quantified manner, and how to efficiently manage and analyze the data for the purpose of fault diagnostics.

3.3 Criterion for Quantitative Classification

In the previous section, a classification method was proposed but there was no specific criterion for classification. Thus, quantified criterion of classification for an optimal diagnostics plan is proposed in this section.

Figure 3-3 shows the distribution of operational data from SCADA of WT. It is seen in Figure 3-3 (a) that power has a dense distribution near the minimum (zero) and the maximum (one). It is also can be seen in Figure 3-3 (b) that rotor speed has a dense distribution near the minimum and maximum (the same as power), and

there is an additional dense group near the cut-in speed, 0.4 in this case. The purpose of the classification is to manage the big data efficiently and design optimal diagnostics plans for each data class. class I and II have relatively small variation of rotor speed which means that computationally efficient diagnostics tools such as order analysis can be used for fault diagnostics. Moreover, it is simpler to utilize the data in class I because we don't need to consider the effect of the torque. Thus, it is reasonable to assign class I as much as possible. Based on this motive, this study attempts to define the criterion for classification to separate the dense group near the maximum of the operational data shown in Figure 3-3. By adopting this concept, we can effectively maximize the opportunity to use cost-effective diagnostics tools using the data in that defined class.

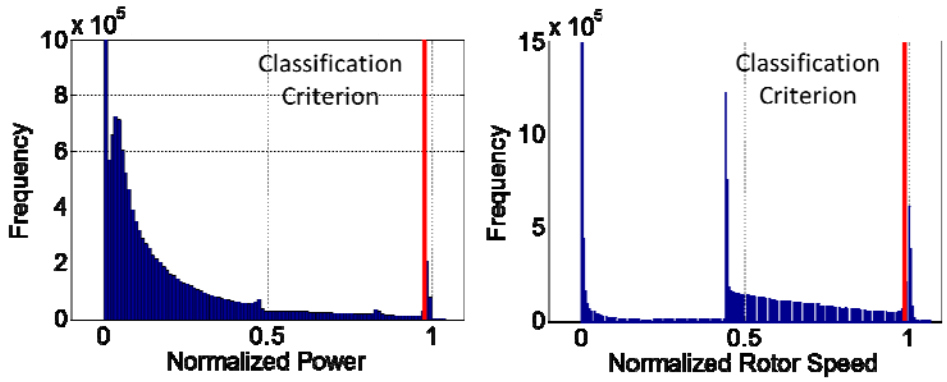

Figure 3-3 Histogram of operational data

(a): Histogram of power, (b): Histogram of rotor speed

In this paper, the inverse cumulative frequency function (Eq.(3.1), Eq.(3.2)) and its primary differential value are employed to separate the dense group. The inverse

cumulative frequency function is the number of samples whose magnitude is larger than a defined value. Thus, the method to separate the dense group can be effectively presented by defining the point that the primary differential value of the inverse cumulative frequency function rapidly decreases.

$$F_c(x_k) = \sum_{k=1}^{N_{bins}} I(x_k \le X_r) \tag{3.1}$$

$$\begin{aligned} I(x) &= 1 \; if \; x \in A \\ &0 \; if \; x \notin A \end{aligned} \tag{3.2}$$

Figure 3-4 to Figure 3-7 illustrate the inverse cumulative frequency function and the primary differential value of power and rotor speed. First, it is clear that the dense distribution near the minimum has an apparent distinction line at exactly zero for both power and rotor speed. Therefore, no guideline is suggested to define the minimum criterion in this study. However, a quantified criterion for the maximum is needed because there is no distinct line near the maximum, as can be seen in Figure 3-4 and Figure 3-6. Thus, the criterion is defined as Eq.(3.3) to capture the point when the rate of change in the inverse cumulative frequency function rapidly decreases.

$$Criterion = \frac{W}{N_{samples}} \sum_{x=c_1}^{c_2} \frac{d(F_c(x))}{dx} \tag{3.3}$$

Threshold means the weight value (W) times the average of the primary differential of the inverse cumulative frequency function from c_1 to c_2 percentile, which is a range where the primary differential value remains almost constant near

the maximum. W, c_1, and c_2 are empirical parameters which may be dependent upon the type of WT. Parameters 5, 0.9, and 0.95 are empirically chosen, respectively, in this research.

Results are summarized in Table 3-1. These results can be combined with the classification method presented at Figure 3-2 to define classes.

Table 3-1 Classification criterion

	Min Criterion	**Max Criterion**
Rotor Speed	0%	98.7%
Power	0%	98%

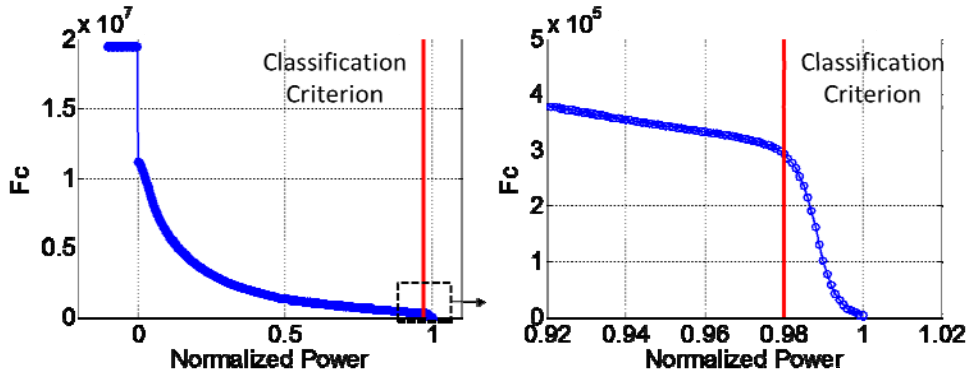

Figure 3-4 Inverse cumulative frequency function (F_c) of power

(a): Over the entire range, (b): Around the maximum

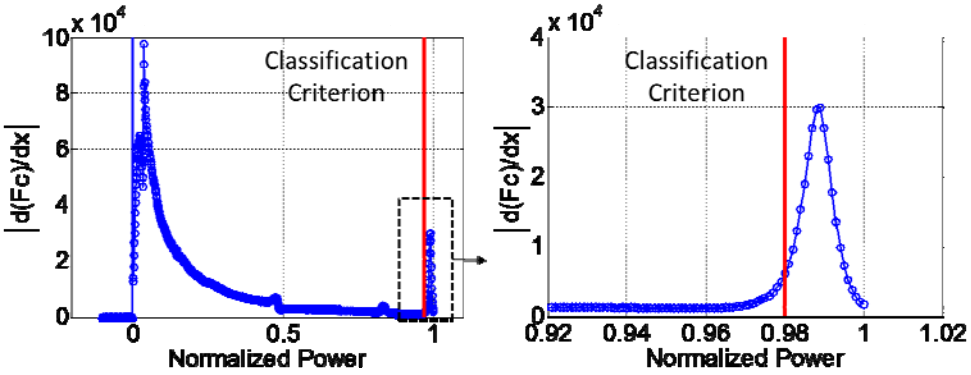

Figure 3-5 Primary differential value of F_c of power

(a): Over the entire range, (b): Around the maximum

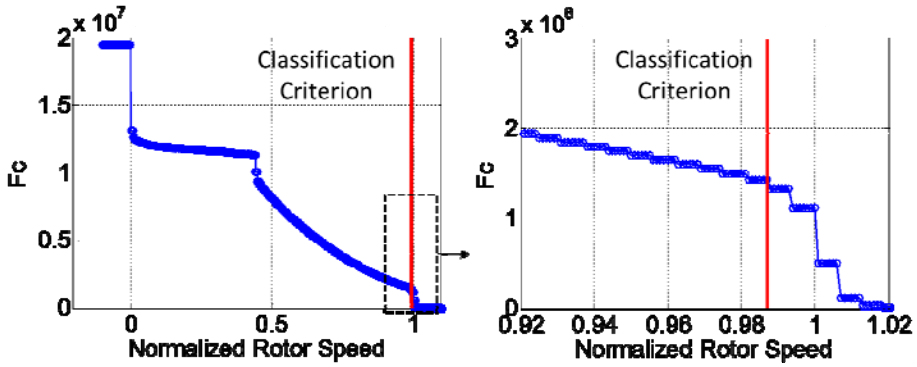

Figure 3-6 Inverse cumulative frequency function (F_c) of rotor speed

(a): Over the entire range, (b): Around the maximum

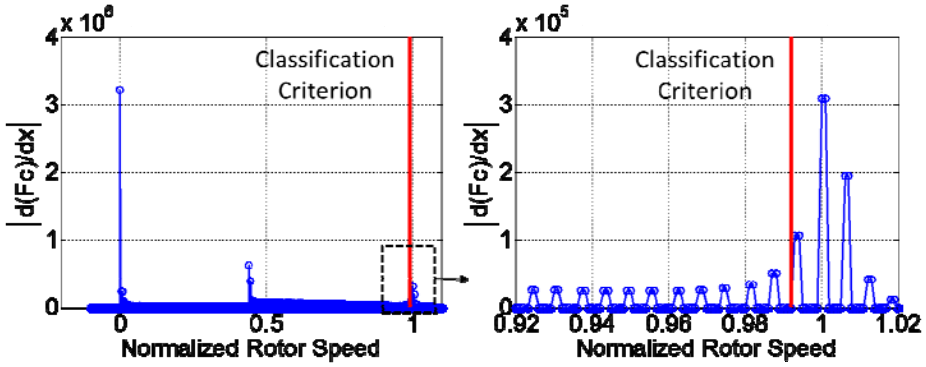

Figure 3-7 Primary differential value of F_c of rotor speed

(a): Over the entire range, (b): Around the maximum

3.4 Diagnostics Plans for the Classes

This study is focused on vibration signals for condition monitoring; however, vibration signals produce the most data and are therefore computationally intensive. Thus, proper condition monitoring strategies should be developed to manage the big data efficiently and enable diagnostics of the WT in real-time. For this purpose, characteristics of each of the defined classes is analyzed and proper diagnostics plans are made in this section.

As can be found in Figure 3-8 (b), most operating data have very clear behavior, generated power has high correlation with rotor speed. Thus it can be identified through the figures that each of the defined classes have their own characteristics. The variation of the data in Figure 3-8 (a) may be caused by uncertainties like sudden strong wind or idle control.

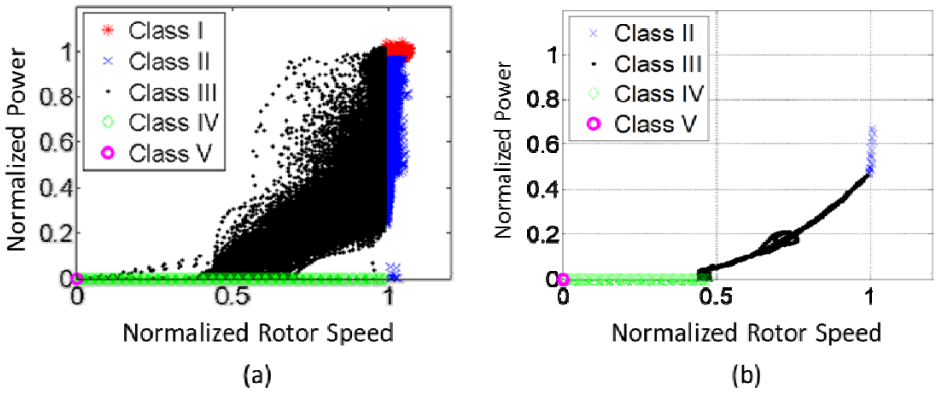

Figure 3-8 Power along with rotor speed with classification

(a) Data for 7 months, (b): Data for one day

Characteristics of each of the defined classes can be analyzed in a statistical manner, as seen in Figure 3-9 and Figure 3-10. Mean, standard deviation (Std.) and CV (Coefficient of Variance) are used for the analysis. Among them, CV which represents the magnitude of fluctuation of the signal is defined as:

$$CV = \frac{Std.}{Mean} \tag{3.4}$$

As you can see, Class I which corresponds to a stationary condition has very low CV of both generated power and rotor speed, as we have estimated. In Class II, CV of rotor speed remains almost zero but CVs of power somehow increases. From this observation, it can be said that diagnostics methods for class I and II can be simplified by using computationally efficient tools which are appropriate for stationary signals, rather than expensive high-tech tools. Order analysis based on ATSA is suggested in this research for diagnostics of WT under class I and II. But power or torque should be considered in class II because vibration is sensitive to applied torque in the rotor system [23].

In class III, power and rotor speed have a relatively high CV value which makes it difficult to use efficient diagnostics methods. Thus, computationally intensive diagnostics techniques such as time-frequency analysis are necessary for this class. In class IV, rotor speed has considerable CV and time-frequency analysis, although difficult, is needed for diagnostics of WT. class V is not significant for the purpose of diagnostics because during class V, the WT is idling and the rotational speed is too low. Phenomenon and diagnostics plans for each class are briefly summarized in Table 3-2.

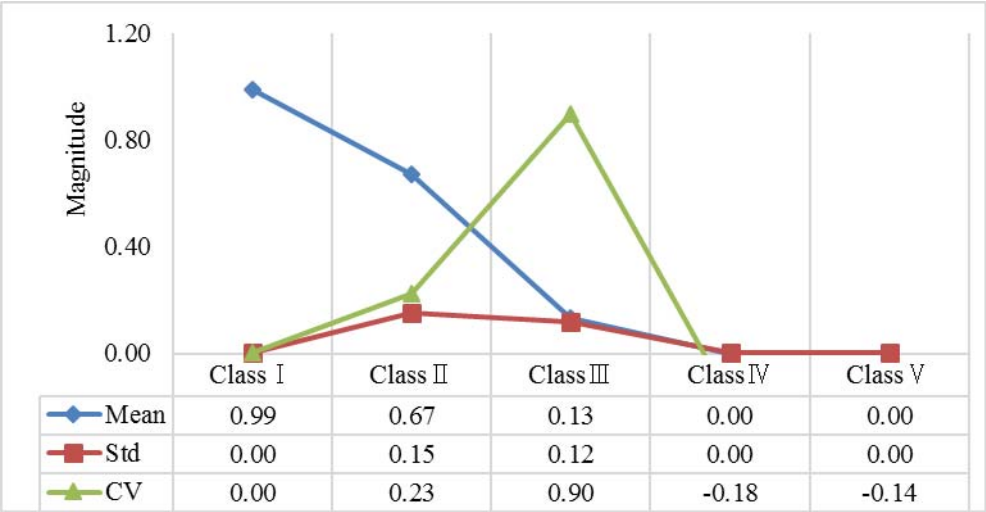

	Class Ⅰ	Class Ⅱ	Class Ⅲ	Class Ⅳ	Class Ⅴ
Mean	0.99	0.67	0.13	0.00	0.00
Std	0.00	0.15	0.12	0.00	0.00
CV	0.00	0.23	0.90	-0.18	-0.14

Figure 3-9 Statistics of power

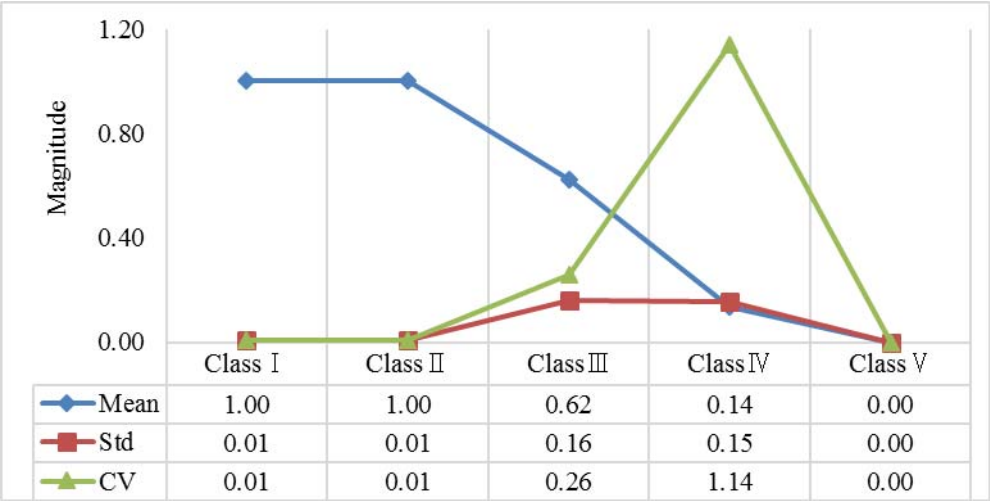

	Class Ⅰ	Class Ⅱ	Class Ⅲ	Class Ⅳ	Class Ⅴ
Mean	1.00	1.00	0.62	0.14	0.00
Std	0.01	0.01	0.16	0.15	0.00
CV	0.01	0.01	0.26	1.14	0.00

Figure 3-10 Statistics of rotor speed

Table 3-2 Diagnostics plan for each class

Class	Phenomenon	Diagnostics plan
I	• Stationary operation state • Power and rotor speed remain nearly unchanged	• Time analysis • Frequency analysis
II	• Quasi-stationary state • Power fluctuates with wind speed under the unchanged rotor speed	• Same as Class I • Power should be considered
III	• Non-stationary state • Power is strongly correlated to rotor speed	• Time-Frequency analysis
V	• Non-stationary state • Transient state before and after idle control	• Difficult (Time-Frequency analysis, if necessary)
IV	• Trivial class • Idling state	• Difficult to analyze the signal

3.5 Results and Discussion

Operation data from WT were classified into four non-trivial condition and one trivial condition. Among non-trivial condition, it was found that two classes corresponding to the stationary and quasi-stationary conditions can be used for diagnostics of WT with computationally efficient diagnostics technique. In this section, distribution of data for defined classes is presented. Figure 3-11 shows percentage of classes using a pie chart. As you can see, class V, which is defined as a trivial class in this study, accounts for 33% of all data. Moreover, if we neglect

the transient region (class IV) which is difficult to analyze, 43% of data can be filtered out. Through these steps, the amount of data to be analyzed can be reduced to 57% of its original size. Class I and II, which correspond to stationary and quasi-stationary conditions, account for only 6% of data. Non-stationary data (Class III) accounts for 51% of the data. Therefore, it is possible to efficiently monitor health of the WT using 6% of data; however, 51% of the data still needs be dealt with in a more complex way.

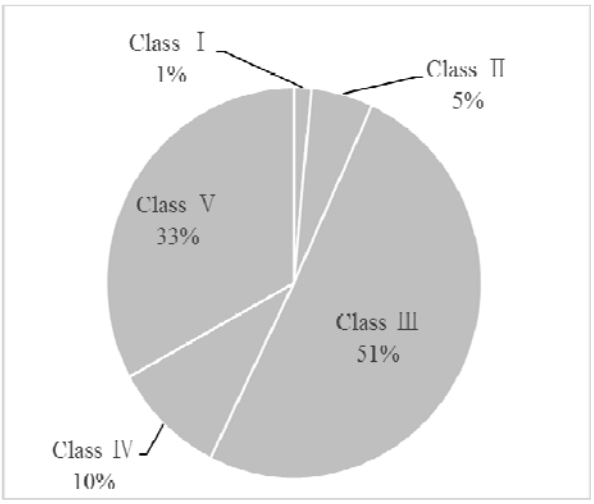

Figure 3-11 Percentage of data in each class

Chapter 4. Autocorrelation-Based Time Synchronous Averaging

Equation Section 4

In this Chapter, the basic concept of time synchronous averaging (TSA) for a rotating system is introduced and then a comparison between some conventional TSA methods for planetary gearboxes is provided. To refine conventional TSA methods, intensive study on kinematics of planetary gearboxes is given and a more efficient method, called autocorrelation-based time synchronous averaging (ATSA), is developed.

4.1 Basic Concept of TSA

Every measured signal has multiple coherent and non-coherent components from various sources. D. Hochmann et al. (2004) attempts to describe the synthesized sensory signal using three main components [24] : synchronous coherent signals ($S(t)$), non-synchronous coherent signals ($N(t)$), and non-coherent random signals ($R(t)$).

$$v(t) = S(t) + N(\mathrm{t}) + R(\mathrm{t}) \tag{4.1}$$

For condition monitoring of a specific sub-system, synchronous coherent signal which is from the sub-system of interest should be separated from the synthesized signal ($v(t)$). TSA has been developed to suppress the non-synchronous coherent signal and the non-coherent random signal and to extract only the synchronous coherent signal.

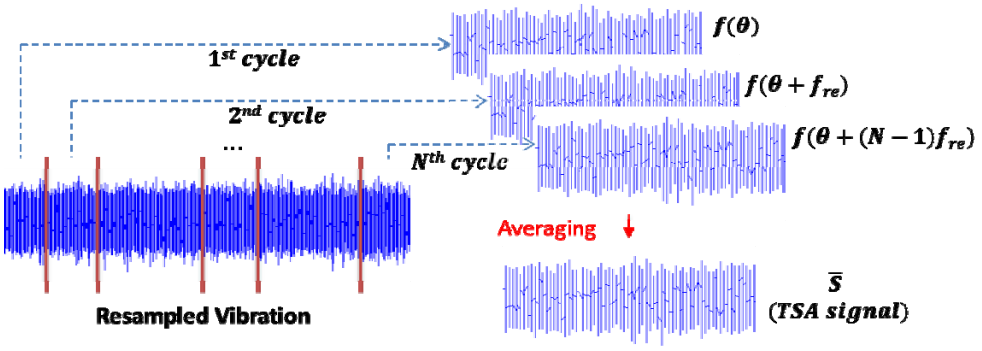

Figure 4-1 Time synchronous averaging of a basic rotating system

The TSA method requires following three main steps.

1) Synchronous resampling of the vibration signal
2) Segmentation of resampled the vibration signal
3) Averaging segmented sets

The basic concept of TSA is to divide the signal into several cyclic segments and then to take their ensemble average. Then, signals out of interest attenuate as the number of segments averaged increases. Before this step, synchronous resampling of the vibration signal is needed because every segmented set should have the same number of sampling points. Moreover, the resampling method enables the signal to be transformed to the angle domain [25].

Let's assume we have rotating system whose rotating speed is increasing as seen in Figure 4-2 (a).

$$t_{n+1} - t_n = constant,\ where\ n\ is\ integer \tag{4.2}$$

$$\theta_{n+1} - \theta_n \neq constant, where\ n\ is\ integer \tag{4.3}$$

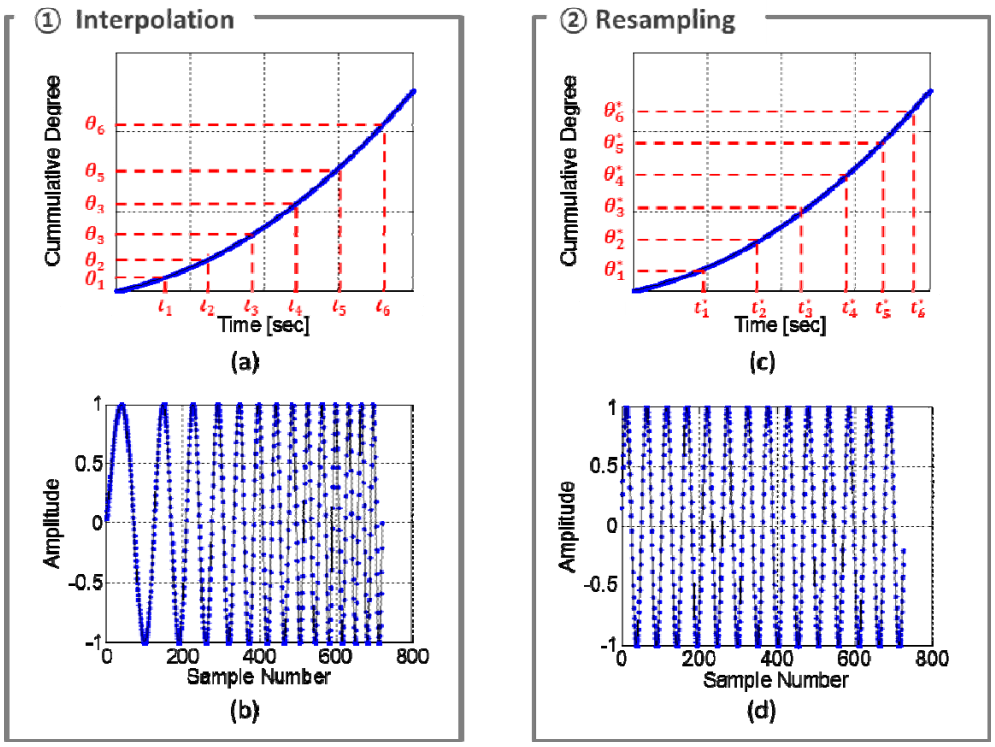

Figure 4-2 Synchronous resampling of the vibration signal

(a): Cumulative degree, (b): Vibration signal,

(c): Resampled cumulative degree, (c): Resampled vibration signal

Notice that the sampling frequency is constant; whereas, the difference between sequentially sampled angles is not constant. The vibration signal caused by a rotating system with increasing speed can be described as Figure 4-2 (b) and it is found that the number of samples in one cycle of the system decreases as the rotating speed increases. This means there is no way to divide the signal into several cyclic sets which have same number of samples and phase. Therefore, the signal requires synchronous resampling. Synchronous resampling is undertaken to interpolate the data to make intervals between the sequentially sampled angles

constant. To make this possible, the system should be equipped with an encoder to exactly catch the points for proper interpolation. An encoder with 60 pulse/rev resolution is used for the research described in this paper.

$$t^*_{n+1} - t^*_n \neq constant,\ where\ n\ is\ integer \tag{4.4}$$

$$\theta^*_{n+1} - \theta^*_n = constant, where\ n\ is\ integer \tag{4.5}$$

After the resampling, we can see that the resampled vibration shows a constant cyclic wave (Figure 4-2 (d)) along with sample numbers, which means that the number of samples in one cycle of the system remains constant. Then resampled vibration can be divided into several segments which have exactly same number of sample points with same phase.

Harry J. Decker and James J. Zakrajsek (1999) performed a comparative study on different interpolation methods for resampling and found that the "cubic spline method does not have considerable increase in accuracy compared to linear interpolation despite it requires significant computation time" [26]. Therefore, the linear interpolation method is employed for resampling in this research.

The number of resampling points for each rotation of the system can be defined as f_{re} and the signal can be divided into several cyclic segments which have f_{re} number of samples. Then, we can separate the synchronous coherent component by ensemble averaging of segmented sets as [27]:

$$\overline{S(\theta)} = \frac{1}{N_{ensemble}} \sum_{n=0}^{N_{ensemble}-1} v(\theta + nf_{re}) \tag{4.6}$$

4.2 Overview of Planetary Gearbox

The basic concept of TSA was presented in the previous section. However, it is difficult to apply the TSA to a planetary gearbox. For the expansion of TSA to a planetary gearbox, the basic structure and principle of mechanical motion of the gearbox should be understood. Figure 4-3 shows the planetary gearbox which was used in this research. The dynamics model for the planetary gearbox was provided by Prof. Choi from Korean Aerospace University (Figure 4-3 (d)). As shown in the figure, the planetary gearbox has 4 main components, including the ring gear, planet gear, sun gear, and carrier. A low-speed shaft (left side in Figure 4-3 (a)) is connected to the carrier and the sun gear operates as the output (right side in Figure 4-3 (a))). The axis of the planet gear is fixed on the carrier and the planet bearing between the planet gear and the carrier enables the planet gear to rotate as you can see in Figure 4-3 (c)).

Figure 4-3 (d) illustrates how the planetary gearbox operates. In the planetary gearbox, the ring gear is fixed at the gearbox housing and inner components rotate as shown in the illustration. The planet gear meshes with the sun gear and the planet gear simultaneously, and there are 6 contacts between inner gears of the gearbox (Figure 4-3 (b), (d)).

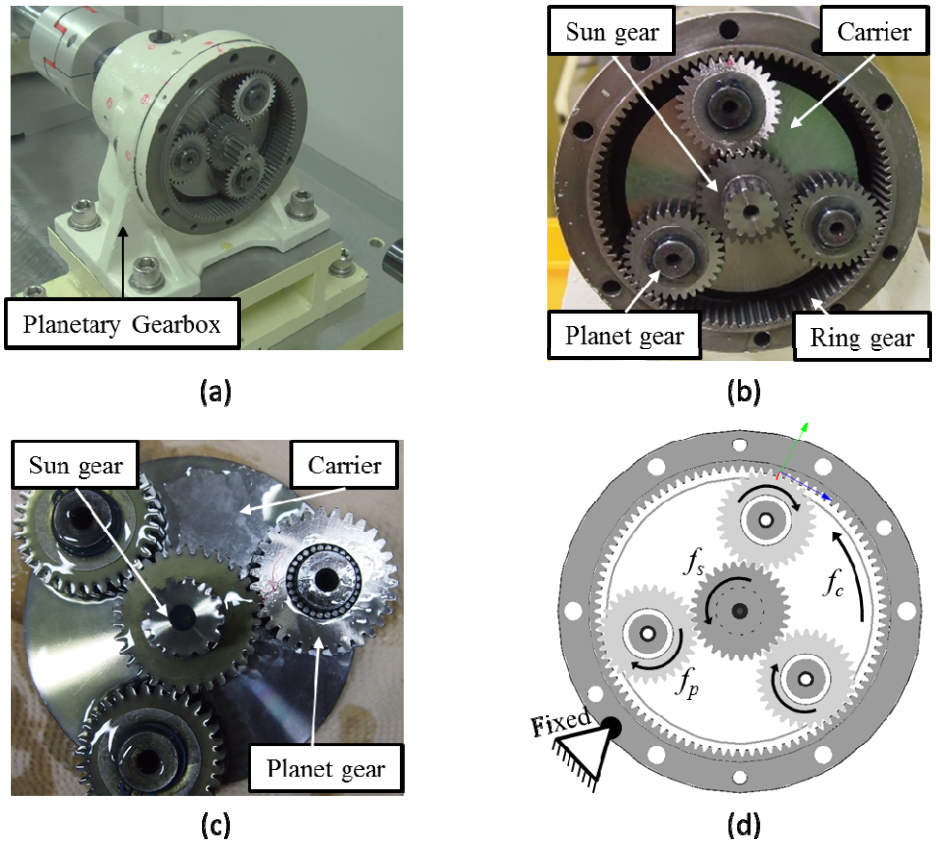

Figure 4-3 Planetary gearbox

(a): Planetary gearbox (side view), (b): Planetary gearbox (front view),

(c): Sun gear, planet gear and carrier, (d): Model of planetary gearbox

All possible rotating frequencies and meshing frequencies of the planetary gearbox that were used in this paper are summarized in Table 4-1. The gear ratio of this planetary gearbox can be calculated as:

$$Gear\ ratio = \frac{N_r + N_s}{N_s} \approx 4.06 \tag{4.7}$$

Table 4-1 Rotating frequency and GMF of the planetary gearbox

Type	Teeth #		Freq.	Equation
Low-speed shaft	-		f_{LSS}	$f_{LSS} = f_c$ (4.8
High-speed shaft	-		f_{HSS}	$f_{HSS} = f_s$ (4.9
Sun gear	N_s=31		f_s	$f_s = f_{HSS}$ (4.10)
Planet gear	N_p=31		f_p	$f_p = f_{pr} - f_c$ (4.11
Ring gear	N_r=95		0	0
Carrier	-		f_c	$f_c = f_s \times \frac{1}{Gear\ ratio} = f_s \times \frac{N_s}{N_r + N_s}$ (4.12
Planet-ring	-		f_{pr}	$f_{pr} = f_c \times \frac{N_r}{N_p}$ (4.13
Planet-sun	-		f_{ps}	$f_{ps} = f_s - f_c$ (4.14
Gear meshing	-		f_{GMF}	$f_{GMF} = N_r f_c = N_p f_{pr} = N_s f_{rs}$ (4.15

An unusual point of the planetary gearbox is that there exists relative motion between the planet gear & the ring gear and the planet gear & the sun gear, expressed as f_{pr} and f_{ps} in Table 4-1. As you can see from the Table 4-1, the gear meshing frequency (GMF) can be described in many ways. If the planet gear is adopted for calculating the GMF, it becomes a function of N_p and f_{pr} which is relative rotational frequency of the planet gear to the ring gear. In this paper, most

description of dynamics of planetary gearbox is based on the relative motion (f_{pr}). If the relative frequency of planet gear to ring gear is not an integer multiple of the carrier frequency, teeth sequence should be considered. Teeth sequence is the number of teeth of the planet gear that are meshing with the ring gear as the planet gear of interest passes the sensor, defined as [28]:

$$P_{n_c,p} = \mathrm{mod}(n_c N_r, N_p) + 1 \tag{4.16}$$

For example, let's assume that tooth number 1 of the planet gear of interest did contact the ring gear at the initial state as shown in Figure 4-4 (a). After 1 rotation of the carrier, tooth number 3, instead of 1, will be meshing with the ring gear, as seen in Figure 4-4 (b). The sequence of teeth in the planetary gearbox which is assembled to the testbed in this research can be arranged as shown in Table 4-2.

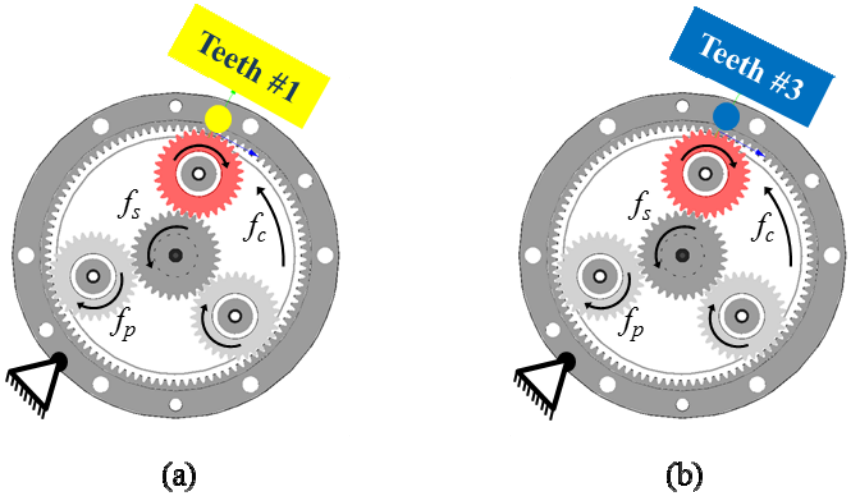

Figure 4-4 Teeth of the planet gear which is meshing with the ring gear
(a): Initial state, (b): After 1 rotation of carrier

Table 4-2 Sequence of the planetary gearbox teeth (1:4.06) in the testbed

n_c	0	1	2	3	4	5	6	7	8	9	10	11	12	13	14	15
$P_{n,p}$	1	3	5	7	9	11	13	15	17	19	21	23	25	27	29	31
n_c	16	17	18	19	20	21	22	23	24	25	26	27	28	29	30	31
$P_{n,p}$	2	4	6	8	10	12	14	16	18	20	22	24	26	28	30	1

Because of this phenomenon, the initial state is made after 31 rotations of the carrier, as can be seen in Table 4-2 at n_c=31. The minimum rotation of carrier needed for it to reset to the initial condition is called the hunting tooth ration (HTR). The HTR can be calculated as [28]:

$$n_{Rest,\mathrm{p}} = \frac{LCM(N_p, N_r)}{N_r} = \frac{31 \times 95}{95} = 31 \tag{4.17}$$

On the other hand, 'hunting tooth cycle (*HTC)'* represents the number of rotation of the carrier until nth reset to the initial position, 31n carrier rotation in this case. Because of the presented characteristics of the planetary gearbox, we are confronted with three main challenges when using TSA for diagnostics of the planetary gearbox [29]. Challenges include:

1) The axis of the planet gears vary with rotation of the carrier
2) Signals are from multiple contacts, including the sun gear & planet gear, and the planet gear & ring gear
3) The meshing condition is not always the same

As the challenges, the rotation of the planet gear makes modulation to vibration. Moreover, vibration by the interesting planet gear can be suppressed by other sources of vibration. Because transducer is fixed on the housing of the gearbox and

the signal is mainly dominated by meshing between the teeth of the planet gear and the teeth of the ring gear just under the transducer [30]. Furthermore, each separated segments cannot be averaged directly because the segmented sets would be under other meshing conditions.

4.3 Conventional TSA for Planetary Gearbox Diagnostics

There have been several attempts to develop a TSA method for use with a planetary gearbox. Prior efforts can be divided into two methods: TSA by McFadden (1991) [29] and the method by Forrester (2001) [31]. Two methods mainly consist of three steps: 1) Extraction of vibration of the planet gear of interest, 2) Mapping the extracted vibration signal into tooth domain and 3) Averaging the mapped signals to separate signals of interest. Other research efforts are not considerably different from these two methods; most have optimized some parameters from one of the two original methods.

McFadden (1986) studied the time domain average of meshing vibration and found that it can help to extract fundamental signals and separate the effect of modulation from the synthesized signal [32]. And modulation of vibration commonly occurs in a planetary gearbox because the axis of the planet gears rotates while the transducer is fixed on the gearbox housing. So, McFadden (1991) expanded his research to examine TSA for a planetary gearbox [31]. A windowing technique was proposed to extract the vibration signal only when the planet gear of interest passes the transducer. Thus, the window function was designed to have a narrow width to cover a few meshing periods as the planet gear is adjacent to the

transducer. Using this technique, the vibration of a specific planet gear in a planetary gearbox can be separated from the synthesized raw signal. Mapping of the windowed signal into tooth domain was also proposed because teeth sequence is not a series of natural numbers, but instead is a set of discrete numbers, defined as Eq.(4.16). Then vibration caused by planet gear of interest can be estimated by ensemble averaging the mapped signals. McFadden (1991) thus used convolution for mapping the windowed signal to the corresponding position of the teeth and averaging them. You can see the graphical illustration of the windowing and mapping procedure in Figure 4-5. The teeth sequence in Table 4-2 is used for the illustration.

Forrester (2001) suggested that the signal should be extracted every time the planet gear meshes with the ring gear [31]. Thus the window function proposed by Forrester (2001) is centered at the point where the planet gear is adjacent to the transducer like the window proposed by McFadden (1991) but covers the entire range of signal, as seen in Figure 4-6. Because every full cycle of the planet gear relative to the ring gear is extracted from the raw signal, the mapping procedure is not required in this method. Thus, vibration of the planet gear of interest can be estimated by averaging the extracted signals as shown in Figure 4-6. Please be careful that every extracted planet cycle should include the effect of the window (even though this is not illustrated in Figure 4-6).

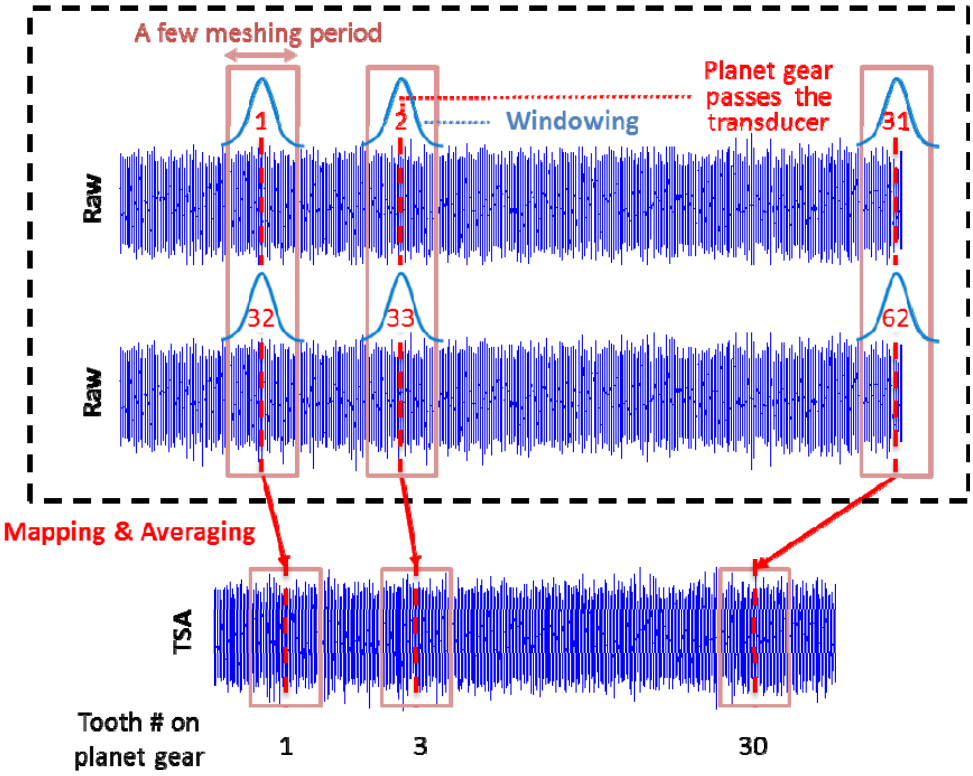

Figure 4-5 Graphical explanation of TSA proposed by McFadden (1991)

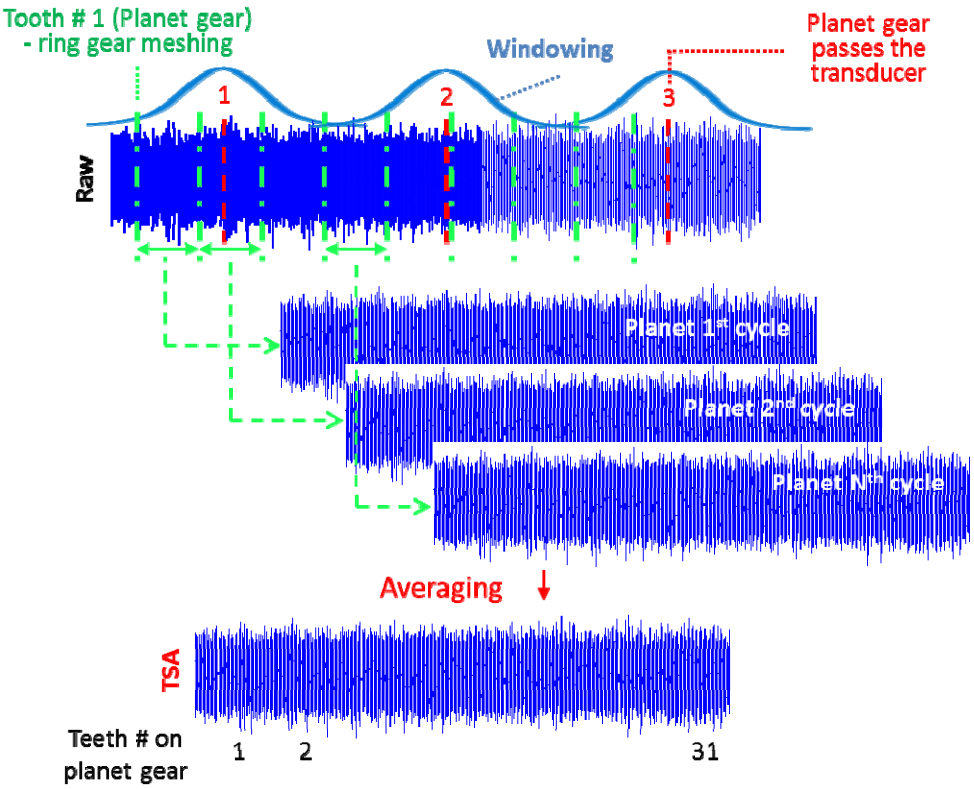

Figure 4-6 Graphical explanation of TSA proposed by Forrester (2001)

Most TSA methods for planetary gearbox developed by other researchers are revised version of TSA by McFadden (1991) and Forrester (2001).

P. D. Samuel et al. (2004) generalized the TSA method by McFadden (1991) and proposed to use an adaptive lifting diagnostics scheme with TSA [28]. Comparative study of the different types and sizes of the windows was given and it was found that a Turkey window which covers 5 teeth with 0.8 of taper steepness performed best among various candidates. Moreover, a feasibility study about usage of multiple sensors for TSA was suggested and presented as an area of future research.

M. R. de Smidt (2009) optimized the size and shape of the Turkey window for TSA by McFadden (1991) [33]. Moreover, an internal vibration monitoring setup for planet gears was developed and TSA by McFadden (1991) was well demonstrated.

Jing Yu (2011) proposed to use the TSA method by Forrester (2001) with wavelet transform for early detection of gear faults [34]. In this thesis, TSA is used for pre-processing of data for diagnostics of WT gearbox.

D. G. Lewicki et al. (2011) modified some parameters in TSA by McFadden (1991), such as the normalization factor, and constructed planet vibration vectors using multiple sensors[35]. The planet vibration vectors constructed are not combined, but rather are used for calculating condition indicators individually.

A. Hood et al. (2011) developed general procedures for practical realization of TSA by McFadden (1991) and described all steps in a graphical manner[36].

4.4 Autocorrelation-based TSA (ATSA)

Two kinds of TSA methods have been developed and revised by several researchers, as presented in previous section. However, it is difficult to apply TSA for condition monitoring of gearboxes in WT because of the following challenges.

First, TSA by McFadden (1991) requires a lot of samples to have enough averaging. However, a stationary signal, which is necessary for robust results of TSA, is rarely acquired in WT—this makes it impossible to attain enough averaging for a robust result. Second, in the case of TSA by Forrester (2001), there is no statistical ground to take the average of signals whenever the planet gear of interest meshes with the ring gear. Therefore, the research outlined in this paper attempts proposes an efficient method for TSA. We call this method autocorrelation-based time synchronous averaging (ATSA). It is designed to use a few stationary signal efficiently by providing statistical ground to take the average of meshing signals based on the autocorrelation function.

For further study on kinematics of planetary gearboxes, the autocorrelation function of the vibration signal is used. The definition of the sample autocorrelation function is the mean value of the signal ($f(t)$) multiplied by itself with time lag τ ($f(t+\tau)$) defined as [37]:

$$R_{vv}(\tau) = E[v(t)v(t+\tau)] \tag{4.18}$$

An autocorrelation function is widely used for understanding characteristics of a system in the time domain instead of the frequency domain. For example, an autocorrelation function of a sine wave with frequency f_0 is a function of the cosine wave with the same frequency f_0. It has zero at 90°of time lag when the shifted sine wave becomes symmetric to the origin with respect to the x-axis. Due to such

characteristics, it is possible to find the pulse repetition interval or period of the original signal using the autocorrelation function. In the example case, it can be found that the sine wave has a frequency of f_0 by the fact that the autocorrelation function (cosine wave) has a local maximum at every multiple of $1/f_0$.

Vibration from the transducer on the planetary gearbox also has a pattern like a sine wave. When we calculate TSA of the vibration signal, similarity of segmented groups should be guaranteed for reasonable averaging. Autocorrelation function of vibration provides statistical way to understand the characteristics of the signal and, furthermore, the similarity of the pattern. This function has high value where similar pattern happens. Then we can adaptively define the points of segmentation of the signal to make the segmented sets have the similar pattern.

Figure 4-7 shows a sample autocorrelation function of vibration from a transducer which is attached to the top of the housing of a planetary gearbox. As the planetary gearbox operates, the meshing condition changes because the axis of planet gears rotates relative to the center of the sun gear. Thus, characteristics of the signal pattern from the fixed transducer would be continuously changing. After 95 rotations of the planet, which is the same as 1 hunting tooth cycle (31 rotations of the carrier) defined in Eq.(4.17), every inner gear resets to the initial position. Then it is estimated that the signal would have very similar pattern to the signal at initial position. As estimated, it is found that a high peak in autocorrelation function exists in Figure 4-7 at n_{pr}=95. This phenomenon can be generalized. If a pattern similar to the initial state happens after x_0 rotations of the planet, the autocorrelation function would have a high value at x_0. As you notice from the figure, the autocorrelation function has peaks at some integer rotations of the planet and has a rule where the peaks have intervals at 3 or 4 rotations of the planet.

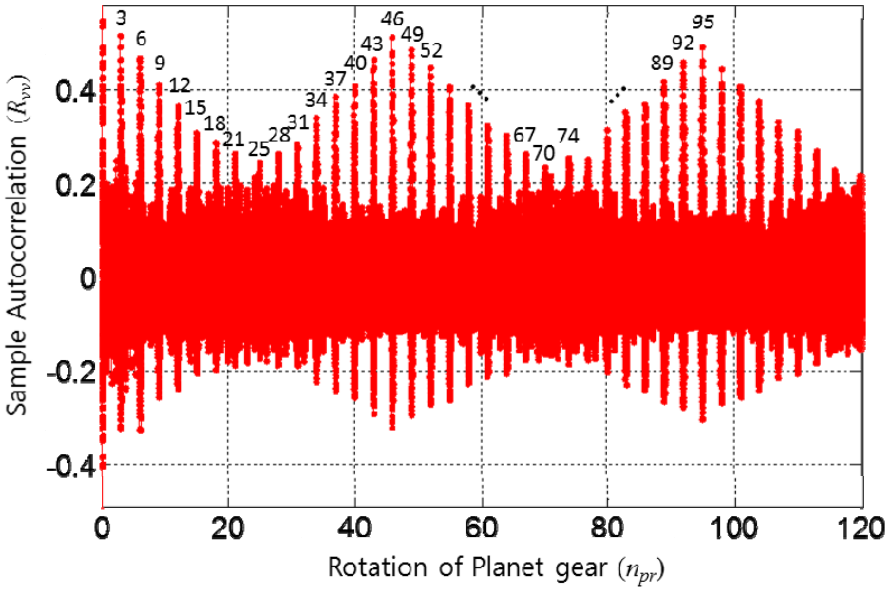

Figure 4-7 Autocorrelation function of vibration from a transducer

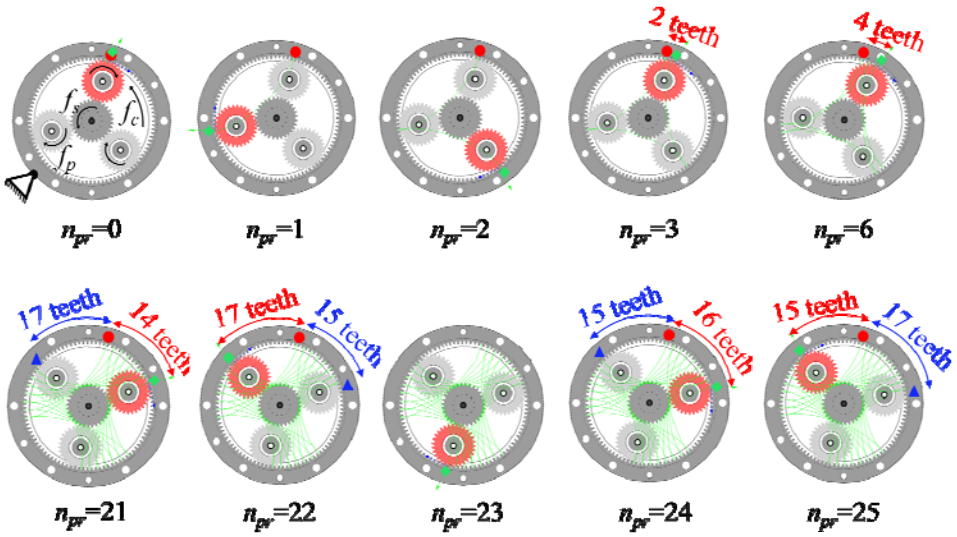

Figure 4-8 Position of inner gears as the planetary gearbox operates

This phenomenon is clearly explained if we look into the inner side of the gearbox (Figure 4-8). Let the blue triangle be a meshing point between the ring gear and the planet gear of interest; let the red circle be the location of the transducer, and let the green diamond be a meshing point between the ring gear and another planet gear. The planet gear of interest is painted red. At the initial state (n_{pr}=0), the planet gear of interest is located under the transducer. Let's assume the tooth number of the planet gear which contacted the ring gear at the initial state was 1, like what is shown in Table 4-2. As the planetary gearbox operates, the axis of the planet gears also rotates. Therefore, the planet gear of interest recedes from the transducer, whereas another planet gear approaches the transducer. After one rotation of the planet gear (n_{pr}=1), another planet gear is almost under the location of the transducer. Therefore vibration is mainly caused by another planet gear and there is no peak in autocorrelation function as shown in Figure 4-7 because the signals have no similar pattern to the signals at initial position. However, as the gearbox continues to operate, the planet gear of interest becomes close to the transducer again. After 3 rotations of the planet gear (n_{pr}=3), the planet gear is near the transducer—as close as two teeth from it. You can also notice that the meshing tooth # of the planet gear after one rotation of the carrier (n_c=1) is 3 according to the sequence of teeth, which is arranged in Table 4-2. You can see from Figure 4-7 that the autocorrelation function is also changing the value corresponding to the rotation of the planet gear. The autocorrelation function has a local maximum at three rotations of the planet gear (n_{pr}=3) because the planet gear becomes close to the transducer again. For more example, the autocorrelation at 24 rotations of the planet gear (n_{pr}=24) has no peak because the planet gear of interest is farther from the transducer than another planet gear, as can be seen in Figure 4-8. Thus, it can be

said that the vibration pattern at 24 rotations of the planet (n_{pr}=24) has no similarity to the signals at the initial state. The peak reappears at n_{pr}=25 because the planet again becomes the closest gear at 25 rotations of the planet gear. It is clearly stated from these observations that the vibration signal would have a similar pattern as long as the planet gear of interest is meshing with the ring gear at close to the transducer.

Notice that TSA by McFadden (1991) extracts the signal only when the planet gear passes the sensor and maps them into the tooth domain for averaging. The averaged signals are from every HTR rotation, which means that we have to wait until high peaks happen at HTC (e.g. n_{pr}=95, 190, … in Figure 4-7) for averaging.

TSA by Forrester (2001) uses all generated signals for averaging with a wide window function. It can be thought that even signals with no peak (e.g. n_{pr}=1, 2, 4, 5, … in Figure 4-7) are used for TSA, although the window function would to some degree take into effect the position of the planet gear of interest.

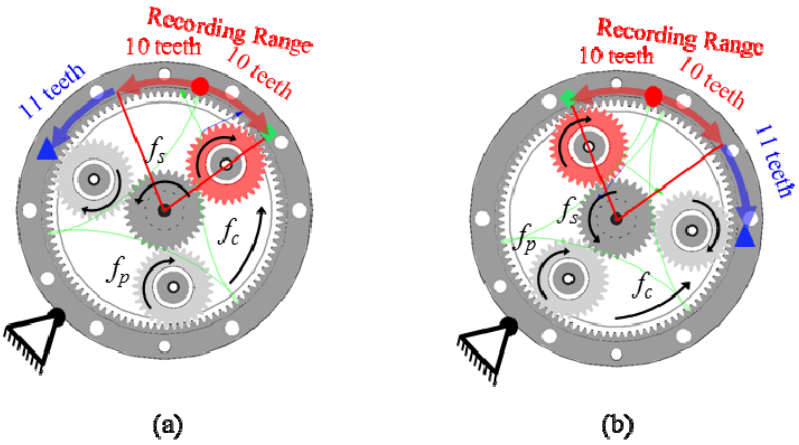

Figure 4-9 Data recording schema for ATSA

(a): Start recording, (b): Finish recording

Thus, autocorrelation-based TSA (ATSA) is proposed in this paper to adaptively take the signals into averaging based on similarity of the vibration pattern. Figure 4-9 is an illustration of the first step of ATSA which is to record the signal when the planet gear of interest is close to the transducer. For robust analysis, a distance within 10 teeth from the transducer is defined as the recording range in this thesis.

The next step is to map the signals into the tooth domain for averaging. Figure 4-10 is an example of the mapping procedure for ATSA. Let's assume the transducer is located on tooth # 1 of the ring gear. Signals are recorded if the planet gear is within the defined recording range (10 teeth from the transducer in this case). Teeth numbers of the planet gear which contacted the ring gear in the range are also recorded. Then the vibration signal is mapped into the tooth domain, according to recorded information about teeth numbers on the planet gear, like shown in Figure 4-10.

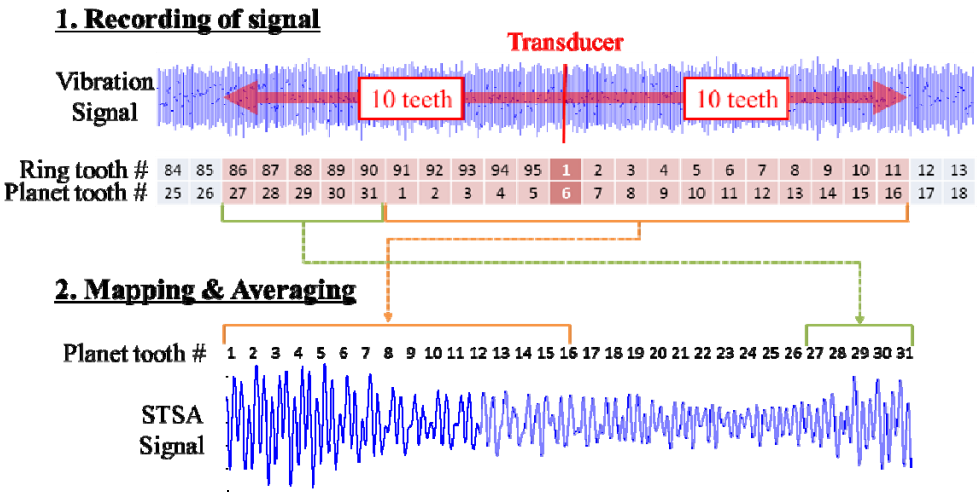

Figure 4-10 Mapping schema for ATSA

This procedure continues during operation of the gearbox, and mapped vibration signals are averaged to make the ATSA signal. Then, ATSA signal can use the scarce stationary signals efficiently than conventional TSA based on statistical grounds which include similarity of the vibration pattern.

4.5 Advantages of ATSA

Forrester (1996) optimized the number of averages of TSA and concluded that 33 averages can effectively remove the signal leakage [38]. D. Lewicki et al. (2011) successfully separated vibration of the planet gear by TSA using data for 20 hunting tooth cycles [35]. However, 20 hunting tooth cycles which correspond to 620 carrier rotations under a stationary condition is not a frequent occurrence in WTs. Approximately 100 seconds of stationary or quasi-stationary data would need to be acquired under 1500rpm of the sun gear in a 4.06:1 gearbox (Figure 4-3) to collect this amount of data. To evaluate the feasibility of TSA for gearboxes in WT and advantages of proposed ATSA, further study on how many useful stationary or quasi-stationary signals can be acquired from WT is performed. Figure 4-11 represents the histograms for duration of data in Class I or Class I & II from a real WT for 7-months. Table 4-3 summarizes the number of cases which remain in the defined class longer than a specific duration. As a result, it can be concluded that it is possible to estimate health of the WT gearbox with enough averaging using TSA by McFadden (1991) 1.5 times a day with only stationary (Class I) data and 11 times a day with stationary plus quasi-stationary (Class I & II) data, provided applied torque is considered for the quasi-stationary data.

ATSA utilizes more data for averaging than conventional TSA. Therefore, ATSA is expected to increase the opportunity to evaluate the system. If results of ATSA using data for 20 seconds have similar accuracy to the results of TSA using data for 60 seconds, ATSA will thus increase the chance to process data more than 10 times compared to TSA. Accuracy of proposed ATSA will be evaluated by comparing health data from TSA in validation chapter.

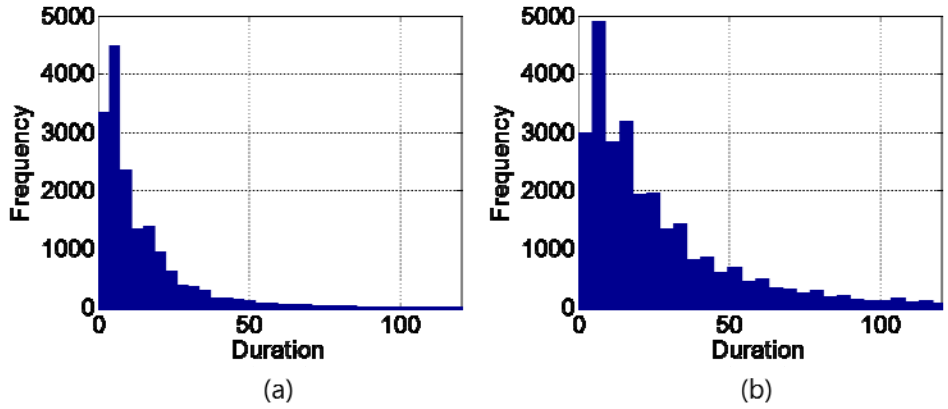

Figure 4-11 Duration of class

(a): Class I, (b): Class I and II

Table 4-3 The number of cases which remain in the defined class longer than a specific duration

Duration [s]	**20**	**40**	**60**	**100**
Class Ⅰ (cases/turbine/1day)	18.7	6.8	3.6	1.5
Class Ⅰ&Ⅱ (cases/turbine/1day)	68.2	35.8	22	11

Chapter 5. Health Data for WT Gearbox Diagnostics

5.1 Review of Health Data for Gearbox Diagnostics

After TSA is obtained from a raw signal, various health data can be calculated. Health data encompasses various values which include information related to the current health state of the system.

Recently, M. Lebold et al. (2000) [39], P. Vecer et al. (2005) [40] and A. Aherwal et al. (2012) [41] reviewed various health data and their characteristics for gearbox diagnostics. J. Zakrajsek et al. (1994) [42], M. Mosher et al. (2002) [43] P. Samuel (2005) [44] studied several useful health data for diagnostics of helicopter transmission which includes a planetary gearbox as a key component. Also, M. Mosher et al. (2002) [43] summarized several health data and suggested their nominal value and threshold value for the purpose of condition monitoring.

M. Lebold et al. (2000) grouped types of vibration into five processing groups as RAW (Raw signal), TSA (Time Synchronous Averaging signal), RES (Residual signal), DIF (Difference signal), BPM (Band pass mesh signal) and then introduced characteristics of each group and corresponding health data [39]. These five groups are involved in this research for summary of the health data and various health data corresponding to the defined groups are arranged based on several papers.

Table 5-1 summarizes the groups and corresponding health data that were employed in this study. Among them, GEN (General group) just means that health data such as RMS, Kurt, CF can be generally obtained from any type of groups such as RAW, TSA, RES, DIF and BPM that are presented by M. Lebold et al.

(2000). For example, FRMS which is obtained by calculating RMS of RES [45], proposed by Y. Lei et al. (2012) will be defined as $RMS_{(RES)}$ in this section instead of by a new name. Most health data are related to the i^{th} statistical moment of the target signal(·) which can be defined as:

$$\mu_{(\bullet),i} = \frac{1}{N_{samples}} \times \sum_{n=1}^{N_{samples}} \left[x_{(\bullet)}(n) - \overline{x_{(\bullet)}} \right]^{i} \tag{4.19}$$

In this section, health data which are summarized in Table 5-1 are reviewed and rearranged in a consistent method. Then, overall procedures for calculation of various health data will be presented.

Table 5-1 List of health data

Group	Health data
GEN	RMS (Root Mean Square), Kurt (Kurtosis), CF (Crest Factor)
RAW (Raw signal)	-
TSA	FM0, SER (Sideband Energy Ratio)
RES (Residual signal)	NA4, NA4*, NA4 reset
DIF a(Difference signal)	FM4, M6A, M8A, ER (Energy Ratio)
BPM (Band pass mesh signal)	NB4

5.1.1 GEN

1) $RMS_{(\bullet)}$

$RMS_{(\bullet)}$ represents the energy of a raw target signal from a system. It doesn't represent the state of each component individually.

$$RMS_{(\bullet)} = \sqrt{\frac{1}{N_{samples}} \times \sum_{n=1}^{N_{samples}} x_{(\bullet)}(n)^2} \tag{4.20}$$

Sometimes, the trend of RMS would be useful information. Thus, delta RMS – which can be obtained by calculating the difference between current RMS and previous RMS – is commonly used for diagnostics of a rotor system.

$$Delta\,RMS = RMS_{(\bullet)}(current) - RMS_{(\bullet)}(previous) \tag{4.21}$$

2) $Kurt_{(\bullet)}$ (Kurtosis)

$Kurtosis_{(\bullet)}$ is the standardized fourth moment of the target signal. Kurtosis represents how the distribution is peaked and the size of its tail. Kurtosis of normal distribution is 3 and this value can be the standard value when it is applied to diagnostics of a gear system.

$$Kurt_{(\bullet)} = \frac{\mu_{(\bullet),4}}{\sigma_{(\bullet)}^{4}} \tag{4.22}$$

3) $CF_{(\bullet)}$ (Crest Factor)

If some defects occur in the gear components, the impact pulse can be observed from the signal. CF measures the maximum size of the impact pulse normalized by its RMS. Lebold et al. (2000) indicate the normal range of CF would reach from 2 to 6 [39].

$$CF_{(\bullet)} = \frac{\max(|x_{(\bullet)}|)}{RMS_{(\bullet)}} \tag{4.23}$$

5.1.2 RAW

RAW is obtained by filtering the noise out from the transducer data. The conditioned signal includes the synchronous coherent signal (*S(t)*), the non-synchronous coherent signal (*N(t)*), and the non-coherent random data signal (*R(t)*) as in Eq.(4.1). B. Wu et al. (2004) suggested to use RAW instead of TSA for diagnostics of a gear system because it seems possible that TSA removes the signals related to defects of the gears [46]. General health data such as RMS, Kurtosis, and Crest Factor can be obtained from RAW.

5.1.3 TSA

TSA ideally contains only the asynchronous coherent signal (*S(t)*) by the effect of TSA. In a planetary gearbox system, the fundamental frequency of the synchronous coherent signal would be near the GMF (Gear Mesh Frequency). Thus, values related to energy of the GMF are calculated in various ways and these values servea to establish the health data.

1) FM0

FM0 is a very simple indicator of the health of a system proposed by Stewart (1977) [47]. It is the magnitude of peak-to-peak of the waveform normalized by the sum of amplitude of the fundamental frequency and their harmonics [39]. M. Alattas et al. (2007) verified it can detect heavy wear and scoring of gears [48].

$$FM0 = \frac{\max(x_{TSA}) - \min(x_{TSA})}{\sum_{i=1}^{N_{harminics}} A(f_i)} \tag{4.24}$$

2) SER

If the defects of a gear become severe, sidebands, amplitude of the fundamental frequency, and their harmonics will increase. Based on this assumption, J. Hanna et al. developed SER [49] which is the magnitude of sidebands normalized by the amplitude of the fundamental frequency. According to the report presented at NREL by S. Sheng (2012), SER can be effectively used for diagnostics of planetary gearboxes of WT [50].

$$SER = \frac{\sum_{i=1}^{N_{sidebands}} A(s_j{}^{f_1})}{A(f_1)} \tag{4.25}$$

5.1.4 RES

RES is calculated by removing fundamental GMF (Gear Mesh Frequency) and their harmonics from TSA. Thus, RES contains information about pure sidebands of the GMF and sidebands of their harmonics. Various health data from RES is very meaningful because a lot of research about diagnostics of gearboxes has focused on monitoring of the amplitude of sidebands.

1) NA4

J. Zakrajsek el al. (1993) developed NA4 to detect progress of severity of the defect. For this purpose, NA4 employs information from previous data records as well as currently acquired data [51]. Information from previous data records is represented by ensemble average of the second moment of previous $N_{ensemble}$ groups.

$$NA4 = \frac{\mu_{(RES),4}}{\left\{ \frac{1}{N_{ensemble}} \sum_{j=1}^{N_{ensemble}} \left[\mu_{(RES_j),2} \right] \right\}^2} \tag{4.26}$$

2) NA4*

H. Decker and J. Zakrajsek (1994) revised the NA4 to reflect the trend of parameters in a statistical manner [52]. The denominator of NA4 is modified to the second moment of RES of a normal gearbox instead of the ensemble average of previous information. The state of the normal gearbox is defined in a quantitative way where "normal" is assigned to the gearbox until the denominator value exceeds the limit defined in [52]. H. Decker and J. Zakrajsek (1994) suggested that the number of samples ($N_{samples}$) for defining the normal state be larger than 30.

$$Limit = \overline{\mu_{(RES),2}} + Z\sqrt{\frac{\mu_{(RES),2}}{N_{samples}}} \tag{4.27}$$

3) NA4 reset

NA4 is more sensitive to applied torque, as well as change of defect, than other health data [53]. Thus, P. Dempsey et al. (2001) proposed NA4 reset to minimize the effect of varying torque [53]. The difference from NA4 is that it resets its denominator when the applied load gets out of the bound which is defined as 10 percent of the current average load.

5.1.5 DIF

As the faults within a gearbox worsen, the magnitude of unexpected frequency becomes large. DIF is obtained from RES by excluding sidebands of fundamental GMF and their harmonics. If we note that RES is obtained by excluding fundamental GMF and their harmonics, it is clear that DIF ideally should not contain any normal vibration components and should have normal Gaussian distribution. Therefore, diagnostics of a gearbox can be performed by tracking the shape and energy of DIF as follows.

1) FM4

Kurtosis originally represents how the distribution is peaked and the size of its tail, as presented earlier and has 3 at normal Gaussian distribution. FM4 can be obtained by calculating the kurtosis of difference signal which should be normal Gaussian noise in the ideal case [47]. Thus, the health state of the gearbox can be estimated by looking into the trend of FM4.

$$FM4 = \frac{\mu_{(\mathrm{DIF}),4}}{\mu_{(\mathrm{DIF}),2}^{\ 2}} \tag{4.28}$$

2) M6A

H. Martin (1989) developed M6A and M8A to detect surface damage of gears [54]. The parameters are a revised version of FM4 where higher moments of the difference signal than ones of FM4 are employed.

$$M6A = \frac{\mu_{(\mathrm{DIF}),6}}{\mu_{(\mathrm{DIF}),2}^{\ 3}} \tag{4.29}$$

3) M8A [54]

$$M8A = \frac{\mu_{(\mathrm{DIF}),8}}{\mu_{(\mathrm{DIF}),2}^{\ 4}} \tag{4.30}$$

4) ER

N. Swansson (1980) proposed ER to use the ratio between the energy of difference signal and a regular signal, such as fundamental frequency, harmonics and their sidebands. P. Samuel et al. (2005) introduced ER and its characteristics. It is said that the energy of difference signal will increase and the amplitude of the regular signal will decrease simultaneously as the "heavy uniform wear" of gears worsen.

$$ER = \frac{RMS_{(DIF)}}{\sum_{i=1}^{N_{harmonics}} \left[A(f_i) + \sum_{j=1}^{N_{sidebands}} A(s_j^{\ f_i}) \right]} \tag{4.31}$$

5.1.6 BPM

Energy of fundamental frequency and their harmonics, including sidebands, is a good indicator of the health state of a gearbox. To consider these values, TSA can be band-passed around fundamental frequency, including sidebands.

1) M6A

J. Zakrajsek (1994) proposed to use amplitudes of fundamental frequency (including their sidebands) as an indicator of the health state of a gearbox [42]. For this purpose, NA4 is modified to have envelope of BPM as the source of the

numerator and denominator as in [39]:

$$NB4 = \frac{\mu_{(E),4}}{\left\{ \frac{1}{N_{ensemble}} \sum_{j=1}^{N_{ensemble}} \left[\mu_{(E_j),2} \right] \right\}^2} \tag{4.32}$$

where E is energy of the Hilbert transform of BPM as in [39], [55]:

$$\mathrm{H}\left[\mathrm{BPM(t)}\right] = \widetilde{BPM}(t) = \frac{1}{\pi} \int_{-\infty}^{\infty} BPM(\tau) \frac{1}{t-\tau} d\tau \tag{4.33}$$

$$E(t) = \sqrt{BPM^2(t) + \widetilde{BPM}^2(t)} \tag{4.34}$$

5.2 Procedures for Calculating Health Data of WT Gearbox

In this section, overall procedures for calculating health data, which are reviewed in the previous section, are presented in a graphical manner, as shown in Figure 5-1.

Step1: Calculate TSA(or ATSA) and transform it to the order domain using FFT (Fast Fourier Transform).

(Health data: FM0 and SER)

Step2: Calculate BPM by applying a band pass filter around the fundamental GMF and their harmonics, including sidebands.

(Health data: NB4)

Step3: Distract GMF and their harmonics from TSA.

Step4: Calculate RES by applying inverse FFT to the signal from Step 3.

(Health data: NA4, NA4 reset and NA4*)

Step5: Distract sidebands of fundamental GMF and their harmonics from RES.

Step6: Calculate DIF by using inverse FFT of the signal from Step 5.

(Health data: FM4, M6A, M8A, ER)

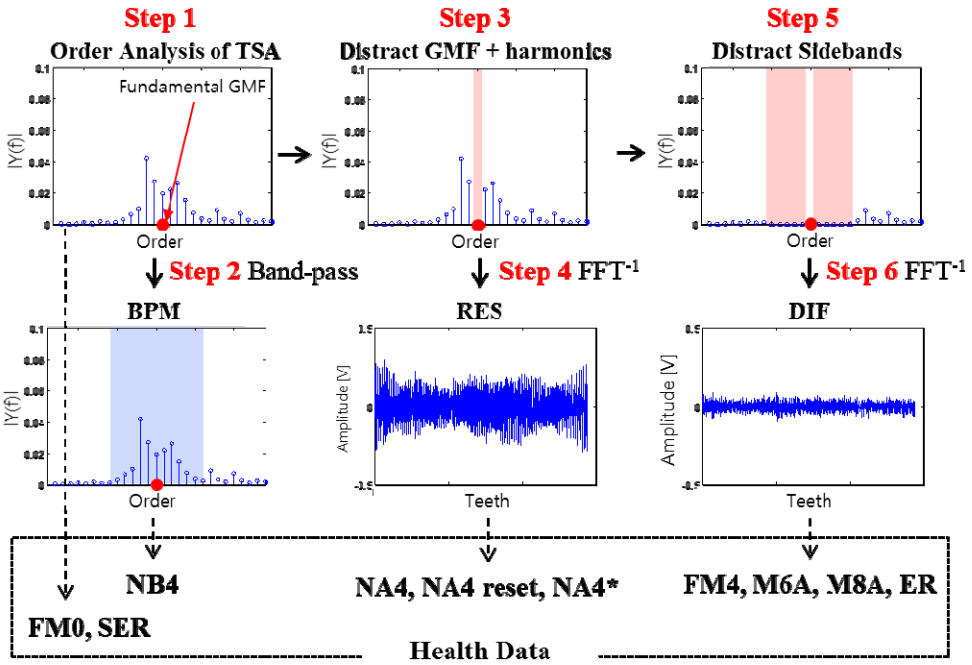

Figure 5-1 Procedures for calculation of health data

Chapter 6. Validation Study for ATSA

6.1 Design of Signal

6.1.1 Design of the Analytical Signal

An analytical signal is employed for validation of the proposed fault diagnostics technique as:

$$v = \sum_{i=1}^{P} v_p a_{pi} + noise_i \tag{4.35}$$

Ideally all planet gears generate the same vibration signals but have a different transfer path according to the position of the planet gears (Figure 6-1 (a)). a_{pi} is accounting for the transfer path of i^{th} planet gear which is a function of the position of that planet gear, as shown in Figure 6-1 (b). The transfer factor a_{pi} will converge to 1 as the planet is adjacent to the sensor, whereas it will attenuate as the planet recedes from the sensor.

$$a_{pi} = (1 + \cos(2\pi(f_c t - (i-1)/3)))/2 \tag{4.36}$$

Noise factor ($noise_i$) can also be employed to express the uncertainty of the gearbox and the trend is vice-versa from the transfer factor (Figure 6-1 (c)), defined as:

$$noise_i = V_{rand} A_{noise} \frac{(1 + 2A_{nosise,min} + \sin(2\pi(f_c t - (i-1)/3 - \pi/2)}{2 + 2A_{nosise,min}} \tag{4.37}$$

Level of minimum and average of the noise is an empirical value and 0.15 and 0.3 are designed in this research respectively.

It is also assumed that an abnormal signal can be described as having a higher amplitude than a normal one when the faulty gear meshes with other gears. In this study, abnormality is added to the vibration of planet 1 (v_1). After all factors are combined as shown in Eq.(4.35), an abnormal condition is invisible in the tooth domain because of the noise, as shown in Figure 6-1 (d).

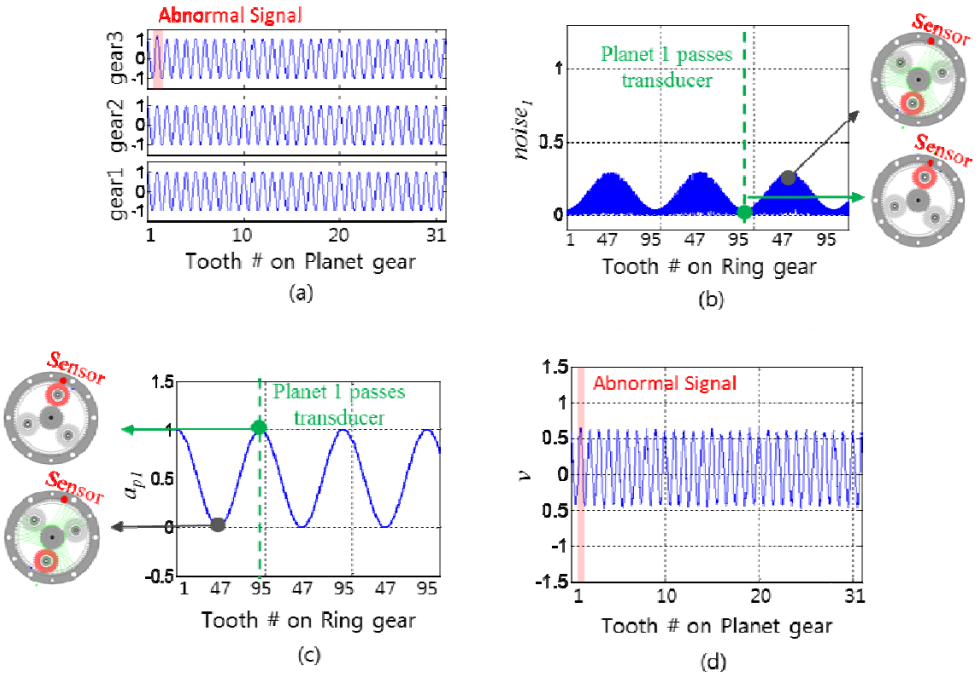

Figure 6-1 Analytical signal

(a): Vibration of individual planet gears, (b): Noise factor of planet gear 1,

(c): Transfer factor of planet gear 1, (d): Combined vibration

6.1.2 Design of Testbed

Absence of normal and abnormal response data from the WT makes it difficult to achieve the objective of this research. Thus, a small scale WT testbed which has similarity to a 2.5MW WT was designed for the research outlined in this paper (Figure 6-2).

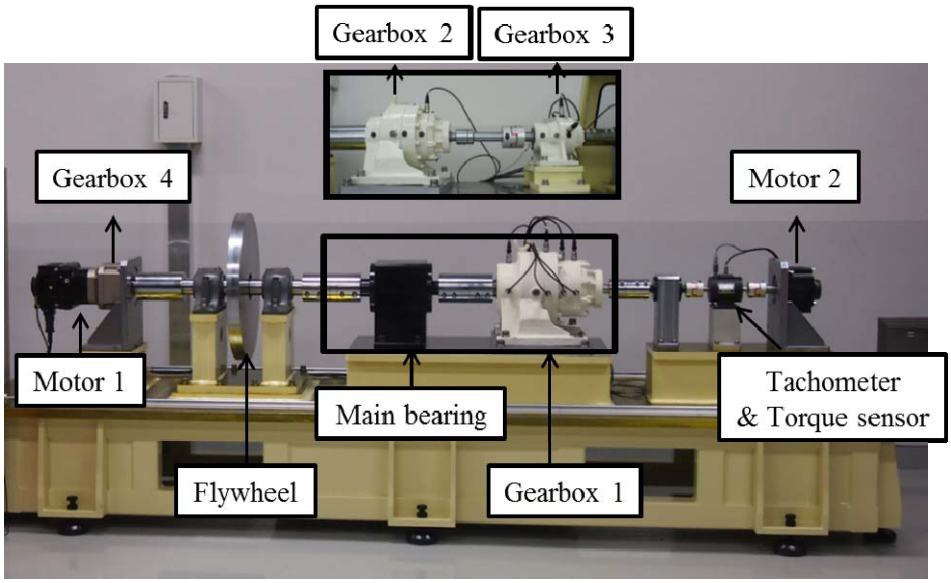

Figure 6-2 Wind turbine testbed

The detailed specifications of the testbed are summarized in Table 6-1.

Gearbox 1, which has 3 stages of planetary gear set can be substituted with gearboxes 2 and 3 which have simpler dynamics characteristics than gearbox 1. Gearbox 3 which has one stage of planetary gear set is to be analyzed in this paper and details are summarized in Table 4-1.

The main considerations for designing the testbed are as follows: The composition is almost identical to that of a WT gearbox so the testbed will have

similarity to a WT. The testbed operates with a closed-loop controller which enables implementation of rotor speed and scaled torque measured from a WT to the testbed. Moreover, this testbed is designed to add artificial defects into the gearbox and bearing. For example, Figure 6-3 shows three levels of artificial cracks in gears which are provided by Prof. Y.H. Jung from Pusan national university [56].

Table 6-1 Specifications of the testbed

Components	Qty.	Specifications
Motor1	1	2kW servo motor
Motor2	1	2kW servo motor
Gearbox 1	1	1:80.47, 3 stage planetary
Gearbox 2	1	1:20.79, 2 stage planetary
Gearbox 3	1	1:4.06, 1 stage planetary
Gearbox 4	1	80:1 reduction gearbox
Main Bearing	1	6218-2z (ball bearing)
Vibe. sensor	8	500mV/g (Range:±10g)
Temp. sensor	4	RTD type
RPM sensor	1	60pulse/rev

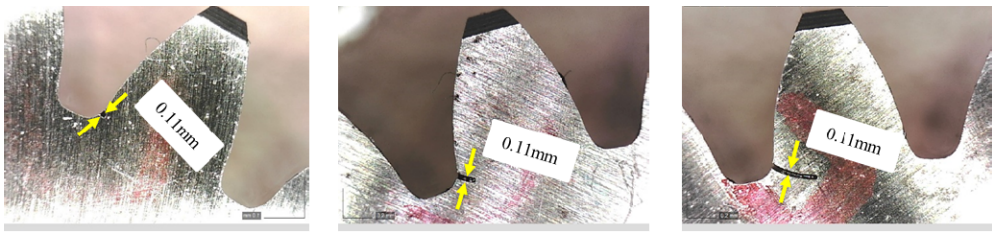

Figure 6-3 Three levels of artificial crack of planet gears

(a): Crack size: 0.1mm, (b): Crack size: 0.44mm, (c): Crack size: 1.1mm

Before the test, the housing of the planetary gearbox was disassembled and every location of contact points of inner gears at the initial state was marked on the components. Every time a test was performed, the inner gears were reset to the initial state. Using these procedures, tests under normal conditions and abnormal conditions or repetitive tests could be performed with the same initial state. During the tests, position of the planet gears could be tracked consistently by using encoder for implementation of TSA or ATSA.

6.1.3 Design of Experiment (DOE)

Experiments are designed to demonstrate the real condition of the WT. DOE is based on testbed and same conditions are made in analytical signals in statistical manner. Rotational speed of the sun gear in the planetary gearbox (1:4.06) was determined as 20 round per seconds (RPS) which is the rated speed of the generator of typical WTs. Applied torque is scaled down to have rated torque which is 4Nm in the testbed. Tests were performed in two ways: 1) for 20 seconds and 2) for 100 seconds. Validation of ATSA using analytical signal is performed by only the case 1 and two of the cases are employed in the testbed.

Each tests is performed for 120 minutes and divided into several data sets with same periods. Design of experiment and corresponding hunting tooth cycle (HTC) are summarized in Table 6-2.

Experiments are performed under both normal and abnormal conditions for each cases. As stated, abnormal condition is defined as a higher peak at the faulted points in the analytical signal. In the testbed, a gear with 1.1mm of artificial crack (Figure 6-3 (c)) is used for demonstrating faulted condition.

Table 6-2 Design of experiments

Case	Data set [sets]	Speed of Sun gear [RPS]	Speed of Sun gear [RPS]	Periods [sec]	Carrier Cycle [cycles]	HTC [cycles]
1	360	20	4.93	20	98	3
2	72	20	4.93	100	492	15

6.2 Results and Discussion

6.2.1 Analytical Signal

For validation of the advantages of ATSA, results from TSA are compared. Test case 1 is used for validation of the proposed diagnostics. First, one example of a residual signal is given in Figure 6-4 to graphically illustrate abnormality in the tooth domain. Residual signal is calculated by excluding fundamental frequency and their harmonics from TSA of ATSA. As shown in Figure 6-4 , An abnormal signal is clearly recognizable in Figure 6-4 (b) whereas cannot be seen in Figure 6-4 (a) because of the noises. Thus it can be concluded that ATSA has an ability to deal with the small amount of data which would not be enough for TSA. Then, among various health data, FM4 and NA4* were used to separate abnormal sets and normal sets, as shown in Figure 6-5. All health data are normalized for easy comparison. As you can see through the figure, abnormal sets are effectively separated from the normal condition using ATSA.

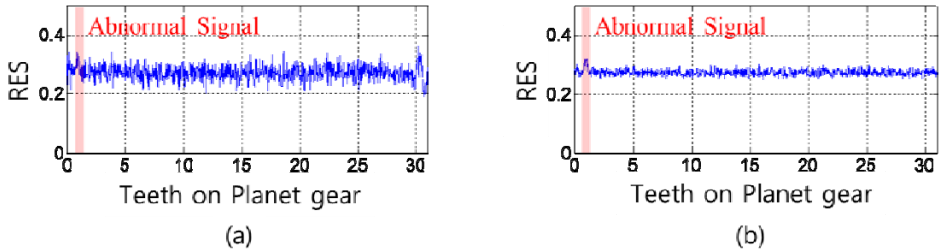

Figure 6-4 Residual signal from an analytical signal for test case 1

(a): Residual by using TSA, (b): Residual by using ATSA

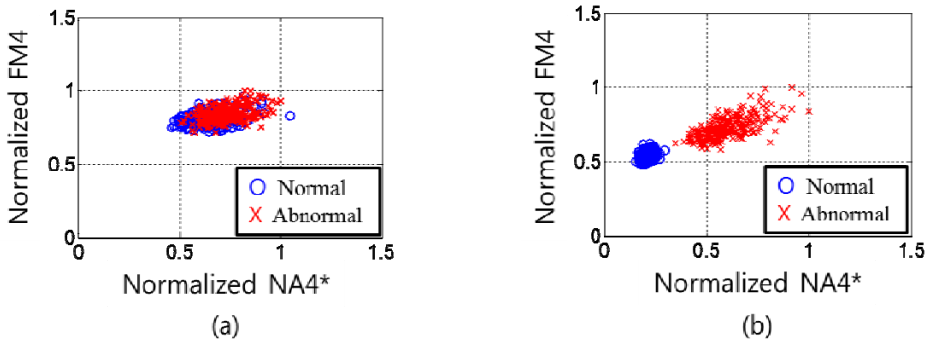

Figure 6-5 Two types of health data for test case 1

(a): Health data using TSA, (b): Health data using ATSA

6.2.2 Testbed Signal

Figure 6-6 shows test results using the proposed diagnostics methods. Frequency analysis of the raw vibration signal is shown in Figure 6-6 (a) and order analysis of the resampled vibration signal is shown in Figure 6-6 (b). Although amplitude of the fundamental gear mesh frequency became large in the order domain than in the frequency domain, there are still other non-synchronous components which may interfere in diagnostics of the planetary gearbox. The noise

components were effectively removed using ATSA. By transforming the ATSA (Figure 6-6 (c)) to the order domain, it is observed that widely distributed noise components were removed from the signal. Moreover, amplitude of fundamental frequency and their harmonics were magnified, as shown in the Figure 6-6 (d). Then, various health data were calculated from the processed signal.

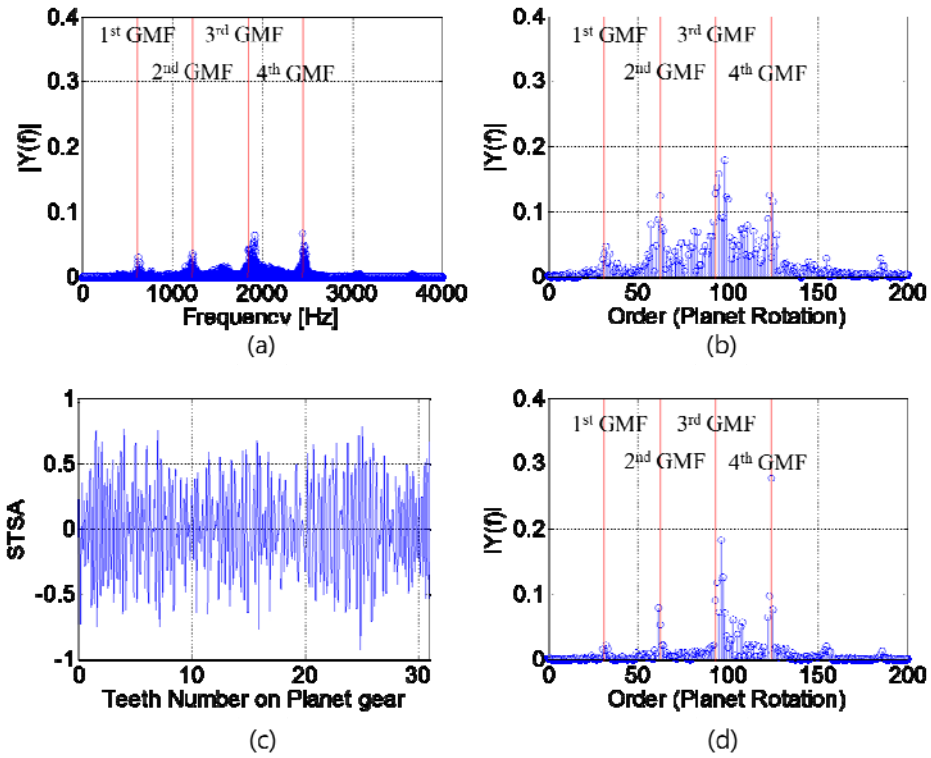

Figure 6-6 Test Results

(a): Frequency analysis, (b): Order analysis of resampled vibration,

(c): ATSA signal and (d): Order analysis of ATSA

In the testbed, it was difficult to see abnormality in the tooth domain using the residual signal. Thus, the trend of health data is used to present the advantage of ATSA in a graphical manner instead of in a residual signal (Figure 6-7 and Figure 6-8). In this paper, 8 health data (HD) are used for representing the trend. Ideally, the trend of health data in a small box should be a smooth line because the data were from a continuous test. As you can see from Figure 6-8, the trend of health data using ATSA does have a smoother pattern with less noise, compared to Figure 6-7 because enough averaging of bigger size of the data was performed. Advantage of ATSA also can be explained by the presented figures. It is can be seen that Figure 6-7 (b) and Figure 6-8 (b) show more reasonable results compared to the results by using TSA (Figure 6-7 (a) and Figure 6-8 (a)). The merits of ATSA which is to extract more data in a limited time than TSA would make the results more robust and reliable.

NA4* and ER were employed among the health data to separate abnormal sets and normal sets, as shown in Figure 6-9 and Figure 6-10. As estimated, abnormal condition were more effectively separated from normal condition when enough averaging were taken. As the two results in Figure 6-9 are compared, advantage of ATSA also can be explained. It is found from the Figure 6-9 (b) that health data calculated from ATSA signal reasonably separate the abnormal and normal condition even using the short period of the data. However, health data calculated from TSA signal with not enough data cannot separated the two conditions definitely.

From the results, it can be concluded that ATSA has an ability to extract more useful data from limited period of the stationary signals.

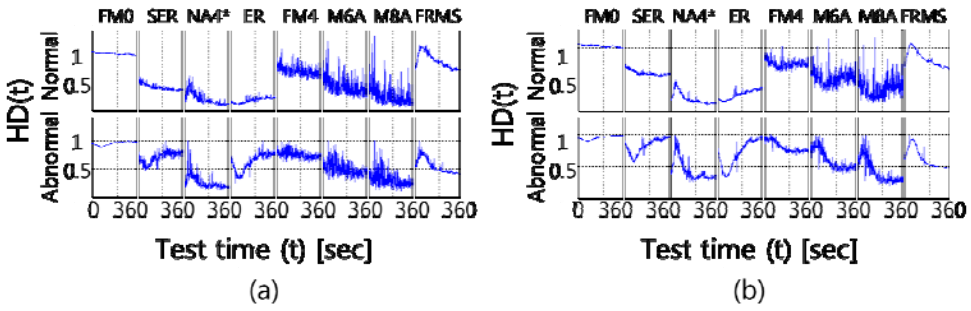

Figure 6-7 Trend of health data (HD) for test case 1

(a): Trend by using TSA, (b): Trend by using ATSA

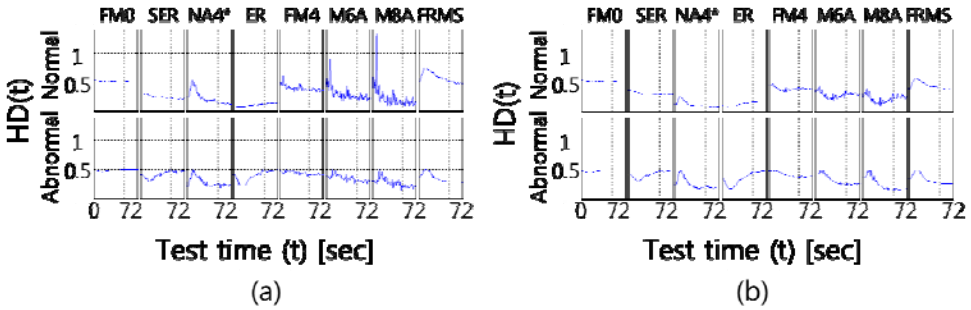

Figure 6-8 Trend of health data (HD) for test case 2

(a): Trend by using TSA, (b): Trend by using ATSA

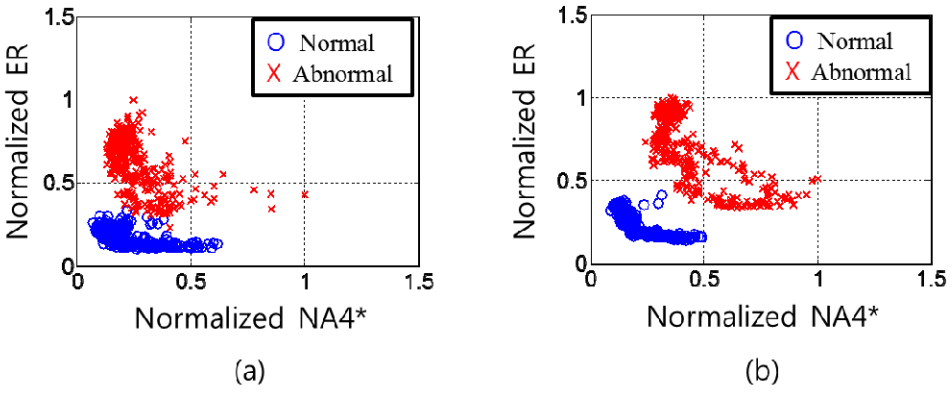

Figure 6-9 Two types of **h**ealth data for test case 1

(a): Health data using TSA, (b): Health data using ATSA

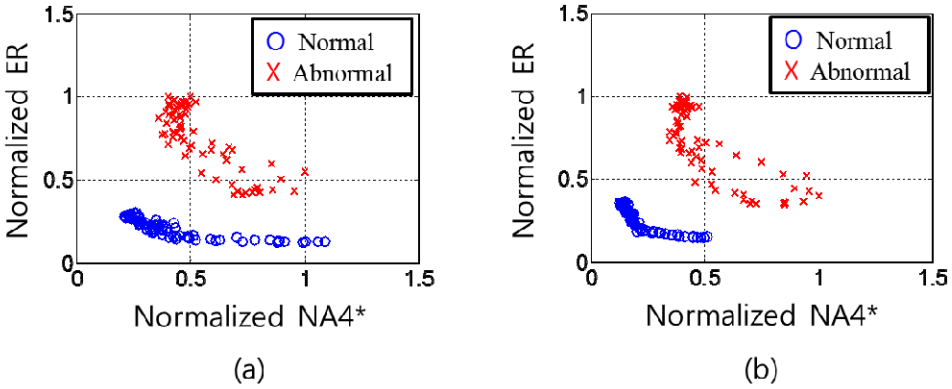

Figure 6-10 Two types of health data for test case 2

(a): Health data using TSA, (b): Health data using ATSA

Chapter 7. Conclusion

7.1 Conclusion

Classification of wind data and diagnostics using stationary data are proposed in this thesis.

In research thrust 1, a huge amount of response data from a wind farm is classified into four non-trivial classes and one trivial class. Characteristics of defined classes are analyzed and optimal diagnostics plans are designed for each class. By classification, 43% of data can be filtered out and only 57% of data needs to be extracted for diagnostics purposes. Among them, Class Ⅰ and Ⅱ, which account for 6% of data, turn out to be adequate for order analysis. The result is a diagnostics method that is computationally efficient.

TSA can be used for pre-processing of order analysis to reduce the noise and make robust and reliable results. However, it is found that Class Ⅰ and Ⅱ which correspond to stationary and quasi-stationary data from a wind farm are not enough for TSA. To overcome this challenge, in research thrust 2, ATSA is proposed to utilize the data more efficiently. ATSA performs an ensemble average of data based on similarity of vibration pattern. Characteristics of similarity of vibration pattern are effectively analyzed using an autocorrelation function.

This thesis also includes the design of an analytical signal and a WT testbed to enable assembly of the main components such as a gearbox or bearing with an artificial fault. In the testbed, a gearbox with one stage of planetary gear set is employed and an artificial crack 1.1mm in size is made on one planet gear.

The validation study was made by using an analytical signal and testbed signals. Among various health data which are presented in this paper, NA4*, FM4 and ER were used for the validation study. The results show that ATSA had better performance when the size of data was not sufficient for conventional TSA.

7.2 Future Research

1) Data Classification

· Optimization of the parameters

Parameters for criterion of classification were empirically chosen. Such parameters include W, c1, and c2 which are used in Eq.(3.3). General values of the parameters which can be used for the classification of data regardless of types of the WTs should be defined.

2) Autocorrelation-based Time Synchronous Averaging (ATSA)

· Optimization of the parameters

Some empirical parameters are employed for demonstration of the ATSA in this thesis. These parameters should be optimized to make the ATSA more powerful diagnostics tool.

(resampling rate, recording range and the number of averaging)

· Multi-axis sensors for ATSA

The merit of ATSA is to effectively utilize scarce stationary data from WT. Another suggestion to collect more data in a limited amount of time is to use multi-axis sensors in one stage of the gearbox. For this purpose, the locations of

planet gears relative to the multiple sensors should be efficiently traced. In addition, a different shape or phase of the vibration pattern from multiple sensors are needed to be adequately adjusted for robust averaging.

- **Validation of ATSA using defined Class I and II**

It is assumed that Class I and II would be appropriate for ATSA because the CV of rotor speed is very low in those classes. Validation using deterministic stationary data was performed in this thesis but the stationary condition or quasi-stationary condition with randomness should be considered for further validation of ATSA in future research. Real WT data can be employed.

- **Machine learning using various health data**

Various types of health data are summarized in this paper, but only a few among them are presented as validation results. Statistical machine learning technique can help us to use all the health data in an efficient way as well as provide us a statistical health index which represents the current state of the system.

3) Time-frequency analysis

Classification of wind data provides a guideline for managing the huge amount of data available from a wind farm and in monitoring the health state of WT. However, 51% of data is still non-stationary data which should be dealt with using computationally intensive diagnostics tools such as time-frequency analysis. Thus, development of computationally efficient time-frequency analysis remain as future research subjects.

Bibliography

1. S. B. Lauha Fried, Shruti Shukla, Steve Sawyer, Sven Teske, “Global Wind Energy Outlook,” 2012.

2. H. Chandler, “Technology Roadmap: Wind Energy,” 2009.

3. Y. Feng, P. J. Tavner, H. Long, and J. W. Bialek, “Review of early operation of UK Round 1 offshore wind farms,” *IEEE PES General Meeting*, pp. 1–8, Jul. 2010.

4. D. Mcmillan and G. W. Ault, “Quantification of Condition Monitoring Benefit for Offshore Wind Turbines,” *Wind Engineering*, vol. 31, no. 4, p. pp 267–285, 2007.

5. D. Z. Chen, Bindi, “Survey of Commercially Available SCADA data Analysis Tools for Wind Turbine Health Monitoring,” 2011.

6. K. Kim, G. Parthasarathy, O. Uluyol, W. Foslien, S. Shuangwen, and P. Fleming, “Use of SCADA Data for Failure Detection in Wind Turbines,” in *2011 Energy Sustainability Conference and Fuel Cell Conference*, 2011, no. October.

7. W. Yang and J. Jiang, “Wind turbine condition monitoring and reliability analysis by SCADA information,” *2011 IEEE*, pp. 1872–1875, Jul. 2011.

8. P. Guo, D. Infield, and X. Yang, “Wind Turbine Generator Condition-Monitoring Using Temperature Trend Analysis,” *IEEE Transactions on Sustainable Energy*, vol. 3, no. 1, pp. 124–133, Jan. 2012.

9. P. Guo and N. Bai, “Wind Turbine Gearbox Condition Monitoring with AAKR and Moving Window Statistic Methods,” *Energies*, vol. 4, no. 11, pp. 2077–2093, Nov. 2011.

10. A. Zaher and Y. Patel, “Online Wind Turbine Fault Detection through Automated SCADA Data Analysis,” *Wind Energy*, no. January, pp. 574–593, 2009.

11. Germanischer Lloyd (GL), “Rules and Guidelines Industrial Services - Guideline for the Certification of Condition Monitoring Systems for Wind Turbines,” 2007.

12. C. J. Crabtree, “Survey of Commercially Available Condition Monitoring Systems for Wind Turbines,” 2011.

13. C. J. Crabtree, Y. Feng, and P. J. Tavner, “Detecting Incipient Wind Turbine Gearbox Failure : A Signal Analysis Method for On-line Condition Monitoring,” *EWEC*, 2010.

14. D. Hochmam and M. Sadok, “Theory of Synchronous Averaging,” *IEEE Aerospace Conference*, pp. 3636–3653, 2004.

15. R. W. Ramirez, *The FFT fundamentals and concepts.pdf*. Tektronix, Inc., 1975.

16. “Understanding FFT Windows,” 2003.

17. B. K. Alsberg, A. M. Woodward, and D. B. Kell, “An introduction to wavelet transforms for chemometricians: A time-frequency approach,”

Chemometrics and Intelligent Laboratory Systems, vol. 37, no. 2, pp. 215–239, Jun. 1997.

18. Z. Hameed, Y. S. Hong, Y. M. Cho, S. H. Ahn, and C. K. Song, "Condition monitoring and fault detection of wind turbines and related algorithms: A review," *Renewable and Sustainable Energy Reviews*, vol. 13, no. 1, pp. 1–39, Jan. 2009.

19. I. Branch, P. Sciences, W. Island, S. Spring, N. Surface, and C. Division, "The empirical mode decomposition and the Hilbert spectrum for nonlinear and non-stationary time series analysis," in *Proceedings of the Royal Society A*, 1998, pp. 903–995.

20. W. Yang, J. Jiang, P. J. Tavner, and C. J. Crabtree, "Monitoring Wind Turbine Condition by the Approach of Empirical Mode Decomposition," in *Proceedings of International Conference of Electrical Machines & Systems*, 2008.

21. W. Yang, R. Court, P. J. Tavner, and C. J. Crabtree, "Bivariate empirical mode decomposition and its contribution to wind turbine condition monitoring," *Journal of Sound and Vibration*, vol. 330, no. 15, pp. 3766–3782, Jul. 2011.

22. H. Mahgoun, R. E. Bekka, and A. Felkaoui, "Gearbox fault diagnosis using ensemble empirical mode decomposition (EEMD) and residual signal," *Mechanics & Industry*, vol. 13, no. 1, pp. 33–44, Apr. 2012.

23. E. M. Huff, M. Field, and M. Mosher, “An Experimental Comparison of Transmission Vibration Responses from OH-58 and AH-1 Helicopters,” in *Americal Helicopter Society 57th Annual Forum*, 2001.

24. D. Hochmam and M. Sadok, “Theory of Synchronous Averaging,” in *2004 IEEE Aerospace Conference Proceedings*, 2004.

25. L. Deyang, “Digital Resampling for Frequency Tracking in Engineering Signal Analysis.pdf,” in *Asia-Pacific Vibration Conference*, 1997.

26. H. J. Decker and J. J. Zakrajsek, “Comparison of Interpolation Methods as Applied to Time Synchronous Averaging,” 1999.

27. T. Barszcz and R. B. Randall, “Application of spectral kurtosis for detection of a tooth crack in the planetary gear of a wind turbine,” *Mechanical Systems and Signal Processing*, vol. 23, no. 4, pp. 1352–1365, May 2009.

28. P. D. Samuel, J. K. Conroy, and D. J. Pines, “Planetary Transmission Diagnostics,” 2004.

29. P. D. McFadden, “A Technique for Calculating the Time Domain Averages of the Vibration of the Individual Planet Gears and the Sun gear in an Epicyclic Gearbox,” *Journal of Sound*, vol. 144, no. 1, pp. 163–172, 1991.

30. Z. Feng and M. J. Zuo, “Vibration signal models for fault diagnosis of planetary gearboxes,” *Journal of Sound and Vibration*, vol. 331, no. 22, pp. 4919–4939, Oct. 2012.

31. B. David Forrester, “Method for the separation of epicyclic planet gear vibration signatures.pdf,” US 6,298,728 B12001.

32. P. D. McFadden, “Examination of a technique for the early detection of failure in gears by signal processing of the time domain average of the meshing vibration,” *Mechanical Systems and Signal Processing*, vol. 1, no. 2, pp. 173–183, Apr. 1987.

33. M. R. de Smidt, “Internal Vibration Monitoring of a Planetary Gearbox,” University of Pretoria, 2009.

34. J. Yu, “Early Fault Detection for Gear Shaft and Planetary Gear Based on Wavelet and Hidden Markov Modeling Early Fault Detection for Gear Shaft and Planetary Gear Based on Wavelet and Hidden Markov Modeling,” University of Toronto, 2011.

35. D. G. Lewicki, R. T. Ehinger, and J. Fetty, “Planetary Gearbox Fault Detection Using Vibration Separation Techniques,” 2011.

36. A. Hood, C. Park, and A. J. Clark, “Sun Gear Fault Detection on an OH-58C Helicopter Transmission,” in *American Helicopter Society 67th Annual Forum*, 2011.

37. J. S. Bendat and A. G. Piersol, *Random Data: Analysis and Measurement Procedures, Fourth Edition*, 4th ed. Hoboken, NJ, USA: John Wiley & Sons, Inc., 2010.

38. B. D. Forrester, “Advanced Vibration Analysis Techniques for Fault Detection and Diagnosis in Geared Transmission Systems,” Swinburne University of Technology, 1996.

39. M. Lebold, K. Mcclintic, R. Campbell, C. Byington, and K. Maynard, “Review of Vibration Analysis Methods for Gearbox Diagnostics and Prognostics,” *Proceedings of the 54th Meeting of the Society for Machinery Failure Prevention Technology*, pp. 623–634, 2000.

40. P. Večeř, M. Kreidl, and R. Šmíd, “Condition Indicators for Gearbox Condition Monitoring Systems,” *Acta Polytechnica*, vol. 45, no. 6, pp. 35–43, 2005.

41. A. Aherwar, “VIBRATION ANALYSIS TECHNIQUES FOR GEARBOX DIAGNOSTIC : A REVIEW,” *International Jouranl of Advanced Engineering Technology*, 2012.

42. J. J. Zakrajsek, “A Review of Transmission Diagnostics Research at NASA Lewis Research Center,” 1994.

43. A. H. P. and E. M. H. M. Mosher, “EVALUATION OF STANDARD GEAR METRICS IN HELICOPTER FLIGHT OPERATION,” *56th Mechanical Failure Prevention Technology Conference*, 2002.

44. P. D. Samuel and D. J. Pines, “A review of vibration-based techniques for helicopter transmission diagnostics,” *Journal of Sound and Vibration*, vol. 282, pp. 475–508, Apr. 2005.

45. Y. Lei, D. Kong, J. Lin, and M. J. Zuo, “Fault detection of planetary gearboxes using new diagnostic parameters,” *Measurement Science and Technology*, vol. 23, no. 5, p. 055605, May 2012.

46. B. Wu, A. Saxena, T. S. Khawaja, R. Patrick, and G. Vachtsevanos, “AN APPROACH TO FAULT DIAGNOSIS OF HELICOPTER PLANETARY GEARS,” in *AUTOTESTCON 2004. Proceedings*, 2004, pp. 475–481.

47. R. M. Stewart, “Some Useful Data Analysis Techniques for Gearbox Diagnostics,” 1977.

48. M. A. Alattas and M. O. Basaleem, “Statistical Analysis of Vibration Signals for Monitoring Gear Condition,” *Damascus Univ. Journal*, vol. 23, no. 2, 2007.

49. J. Hanna, C. Hatch, M. Kalb, A. Weiss, and H. Luo, “Detection of Wind Turbine Gear Tooth Defects Using Sideband Energy Ratio ™,” in *China Wind Power 2011*, 2011.

50. S. Sheng, “Wind Turbine Gearbox Condition Monitoring Round Robin Study – Vibration Analysis,” NREL, 2012.

51. J. J. Zakrajsek, D. P. Townsend, and H. J. Decker, “An Analysis of Gear Fault Detection Methods as Applied to Pitting Fatigue Failure Data,” 1993.

52. H. J. Decker, R. F. Handschuh, and J. J. Zakrajsek, “An Enhancement to the NA4 Gear Vibration Diagnostic Parameter,” 1994.

53. P. J. Dempsey and J. J. Zakrajsek, “Minimizing Load Effects on NA4 Gear Vibration Diagnostic Parameter,” in *Proceedings of the 55th Meeting of the Society for Machinery Failure Prevention Technology*, 2001.

54. H. R. Martin, “Statistical Moment Analysis as a Means of Surface Damage Detection,” in *Proceedings of the 7th International Modal Analysis Conference*, 1989.

55. M. Feldman, “Hilbert transform in Vibration Analysis,” *Mechanical Systems and Signal Processing*, vol. 25, no. 3, pp. 735–802, Apr. 2011.

56. Y. H. Jung, J. D. Yun, S. H. Lee, and J. H. Fu, “Mechinical Fault Imbedding Process for Major Mechanical Parts of Offshore Wind Turbine,” in *Proceedings of the Korean Society of Mechanical Engineers 2012 Spring Annual Meeting*, 2012, pp. 159–160.

국문 초록

최근 풍력발전기의 신뢰성 문제가 풍력에너지 산업에서 큰 이슈가 되고 있다. 특히 풍력발전기의 기어박스는 유지보수 비용이 크기 때문에, 풍력발전기의 부품 중에서 경제적 위험도가 가장 크다고 평가되고 있다. 지금까지 풍력발전기의 신뢰성을 보장하기 위한 수많은 연구가 진행되었음에도 불구하고, 아직까지 해당 연구 분야는 여러 가지 어려운 문제점에 직면해 있다. 대표적으로 크게 1) 비정상 (non-stationary) 운행 상태로 인해 발생하는 고장진단 기술의 어려움, 2) 특정 풍력발전 단지 내에 수많은 센서로부터 계측되는 방대한 양의 데이터와 등으로 나눌 수 있다.

따라서 본 연구에서는 일반적인 고장진단 과정을 포괄하는 기어박스의 고장진단 프레임워크를 제안한다. 제안된 프레임워크는 방대한 양의 데이터를 효율적으로 관리하는 동시에 정확한 고장진단 기술의 적용을 가능케 한다. 이를 위해 본 학위논문은 1) 풍력발전 운행 데이터의 분류 시스템 개발, 2) 진동기반 고장진단 기술 개발로 구성되어 있다.

첫 번째 연구에서는, 방대한 양의 풍력발전 데이터를 해당 풍력발전기의 거동 특성 (로터 회전 속도, 발전량)에 의거하여 유의미한 네 가지 (Class I. stationary; Class II. quasi-stationary; Class III. non-stationary with high correlation; Class IV. non-stationary with no correlation) 클래스와 무의미한 한 가지 (Class V. idle) 클래스로 분류한다. 이후 각 클래스에 해당하는 데이터의 특성에 기반하여 최적의 고장진단 계획을 설계한다. 데이터 분류기법 개발을 위해 영흥 풍력단지로부터 취득한 풍력발전기의 거동 정보를 이용하였다.

두 번째 연구에서는 정의된 클래스 중 두 가지 클래스 (Class I & II)를 토대로 진동기반 고장진단 기술을 개발한다. 고장진단 기술은 보통 신호의 노이즈를 제거하기 위한 시간 동기 평균화 (Time synchronous averaging)과 유의미한 건전성 데이터를 추출하기 위한 오더분석으로 구성될 수 있다. 하지만 풍력발전기의 유성기어박스의 경우 내부에 포함되어 있는 여러 기어들의 복합적인 작용과 더불어 유성 기어의 축이 계속적으로 변하는 문제가 발생하기 때문에 기존의 고장진단 방법을 적용할 수 없다. 따라서 이 논문에서는 풍력발전기의 유성 기어박스에 대한 고장진단을 위해 새로운 시간 동기 평균화 방법인 자기상관함수 기반 시간동기 평균화 (Autocorrelation-based time synchronous averaging) 기법을 개발하였다.

제안된 진동기반 고장진단 기법을 검증하기 위해서 두 가지 신호(수학적 신호, 테스트베드로부터 취득한 신호)가 사용되었다. 이를 위해 우선 두 개의 모터와 메인 베어링, 플라이휠, 기어박스 그리고 13개의 센서 시스템이 구축되어 있는 2kW 풍력발전기 테스트베드가 설계되었다. 특히 인위적 고장이 인가된 기어가 기어박스에 조립될 수 있도록 설계되어 고장진단 연구에 활용할 수 있도록 하였다. 그리고 해당 테스트베드의 거동을 수학적 신호(analytical signal)로 표현하여 고장진단 기법을 사전 검증하였다.

정상 (healthy) 기어박스와 고장(faulty) 기어박스로부터 취득한 신호를 분석하기 위해 자기상관함수 기반 시간동기 평균기법과 오더 분석법을 사용한 결과 제안된 고장진단 기법은 정상 (healthy) 신호와 고장(faulty) 신호를 잘 구별할 수 있었다.

주요어: 풍력 발전기 기어박스
상태 감시
고장 진단
유성 기어
건전성 데이터
시간 동기 평균
운행 데이터 분류

학 번: 2011-23346

감사의 글

세상에는 알아가고 싶은 일들이 너무나 많습니다. 그 중 학부를 졸업할 무렵 가장 알고 싶었던 기계공학에 대해 공부를 하고자 대학원에 입학한지 2년이라는 시간이 흘렀습니다. 공학도로서 최소한의 자질을 갖추기 위해 공부했던 2년이라는 시간은 결코 긴 시간이 아니었습니다. 공부를 하는 동안 저에게는 이전보다 더 큰 호기심과 배움에 대한 욕구가 가득 차게 되었습니다.

우선 저에게 이러한 마음을 갖게 해주신 윤병동 교수님께 진심으로 감사의 말씀을 전해 드리고 싶습니다. 교수님께서 저희가 공부를 하고 인생을 살아가는 데 있어서 꼭 필요한 주옥 같은 말씀들을 해 주실 때마다, 그리고 저를 비롯한 연구실의 모든 학생들을 대하시는 교수님의 진실된 모습을 볼 때마다 저는 힘을 얻고 앞으로 나아갈 수 있었습니다. 앞으로 공학도로서의 삶을 살아갈 때 항상 교수님의 가르침을 마음에 새기고 올바른 길을 걸어갈 수 있도록 노력하겠습니다. 또한 논문의 심사를 위해 귀중한 시간을 허락해 주신 김윤영 교수님과 김도년 교수님께도 감사의 말씀을 전해 드립니다.

그리고 시스템 건전성 및 위험도 관리 연구실 식구들에게도 감사할 일들이 너무도 많습니다. 가족 같은 분위기에 항상 웃음으로 저를 대해 주시는 여러분이 있어 행복한 시간을 보낼 수 있었습니다. 또한 연구를 수행하는 데 있어 진심 어린 충고를 아끼지 않고 해주신 모든 식구 여러분께 정말 감사 드립니다. 이 논문은 여러분들이 없었다면 결코 완성되기가 쉽지 않았을 것입니다.

마지막으로 몸소 사랑을 실천해 주시고 올바르게 살아가는 방법을 보여 주시는 우리 부모님과 누나, 감사합니다. 저에게 주시는 크나큰

사랑으로 인해 저는 삶을 살아갈 힘을 얻습니다. 집을 떠나 타지생활을 하는 중에도 저에게는 단 한번도 가족의 사랑이 느껴지지 않았던 순간이 없었습니다. 삶의 표본을 보여주시는 어머니, 아버지, 그리고 부모님의 사랑에 보답하여 효도하고 있는 누나, 사랑합니다.

제 삶의 목표는 제가 받아온 엄청난 사랑을 모두에게 나누는 것입니다. 세상을 힘들게 살아가고 있는 불우한 우리의 이웃들과 조금의 사랑과 관심이 필요한 우리 아이들에게 제가 받은 사랑을 베풀 수 있는 사람이 될 수 있도록 노력하겠습니다.

본 연구는 한국에너지기술평가원 에너지 국제공동연구 사업(0420-20120138)으로 이루어진 것으로, 본 연구를 가능케 한 평가원 및 관계자 여러분께 감사 드립니다.